IEC TR 61282-13

Edition 1.0 2014-05

TECHNICAL REPORT

colour inside

Fibre optic communication system design guides – Part 13: Guidance on in-service PMD and CD characterization of fibre optic links

IEC TR 61282-13:2014-05(en)

IEC Central Office
3, rue de Varembé
CH-1211 Geneva 20
Switzerland

Tel.: +41 22 919 02 11
Fax: +41 22 919 03 00
info@iec.ch
www.iec.ch

About the IEC
The International Electrotechnical Commission (IEC) is the leading global organization that prepares and publishes International Standards for all electrical, electronic and related technologies.

About IEC publications
The technical content of IEC publications is kept under constant review by the IEC. Please make sure that you have the latest edition, a corrigenda or an amendment might have been published.

IEC Catalogue - webstore.iec.ch/catalogue
The stand-alone application for consulting the entire bibliographical information on IEC International Standards, Technical Specifications, Technical Reports and other documents. Available for PC, Mac OS, Android Tablets and iPad.

IEC publications search - www.iec.ch/searchpub
The advanced search enables to find IEC publications by a variety of criteria (reference number, text, technical committee,…). It also gives information on projects, replaced and withdrawn publications.

IEC Just Published - webstore.iec.ch/justpublished
Stay up to date on all new IEC publications. Just Published details all new publications released. Available online and also once a month by email.

Electropedia - www.electropedia.org
The world's leading online dictionary of electronic and electrical terms containing more than 30 000 terms and definitions in English and French, with equivalent terms in 14 additional languages. Also known as the International Electrotechnical Vocabulary (IEV) online.

IEC Glossary - std.iec.ch/glossary
More than 55 000 electrotechnical terminology entries in English and French extracted from the Terms and Definitions clause of IEC publications issued since 2002. Some entries have been collected from earlier publications of IEC TC 37, 77, 86 and CISPR.

IEC Customer Service Centre - webstore.iec.ch/csc
If you wish to give us your feedback on this publication or need further assistance, please contact the Customer Service Centre: csc@iec.ch.

IEC TR 61282-13

Edition 1.0 2014-05

TECHNICAL REPORT

colour inside

Fibre optic communication system design guides – Part 13: Guidance on in-service PMD and CD characterization of fibre optic links

INTERNATIONAL ELECTROTECHNICAL COMMISSION

PRICE CODE X

ICS 33.180.01

ISBN 978-2-8322-1572-2

CONTENTS

INTERNATIONAL ELECTROTECHNICAL COMMISSION

_____

FIBRE OPTIC COMMUNICATION SYSTEM DESIGN GUIDES –

Part 13: Guidance on in-service PMD and CD characterization of fibre optic links

FOREWORD

1) The International Electrotechnical Commission (IEC) is a worldwide organization for standardization comprising all national electrotechnical committees (IEC National Committees). The object of IEC is to promote international co-operation on all questions concerning standardization in the electrical and electronic fields. To this end and in addition to other activities, IEC publishes International Standards, Technical Specifications, Technical Reports, Publicly Available Specifications (PAS) and Guides (hereafter referred to as "IEC Publication(s)"). Their preparation is entrusted to technical committees; any IEC National Committee interested in the subject dealt with may participate in this preparatory work. International, governmental and non-governmental organizations liaising with the IEC also participate in this preparation. IEC collaborates closely with the International Organization for Standardization (ISO) in accordance with conditions determined by agreement between the two organizations.
2) The formal decisions or agreements of IEC on technical matters express, as nearly as possible, an international consensus of opinion on the relevant subjects since each technical committee has representation from all interested IEC National Committees.
3) IEC Publications have the form of recommendations for international use and are accepted by IEC National Committees in that sense. While all reasonable efforts are made to ensure that the technical content of IEC Publications is accurate, IEC cannot be held responsible for the way in which they are used or for any misinterpretation by any end user.
4) In order to promote international uniformity, IEC National Committees undertake to apply IEC Publications transparently to the maximum extent possible in their national and regional publications. Any divergence between any IEC Publication and the corresponding national or regional publication shall be clearly indicated in the latter.
5) IEC itself does not provide any attestation of conformity. Independent certification bodies provide conformity assessment services and, in some areas, access to IEC marks of conformity. IEC is not responsible for any services carried out by independent certification bodies.
6) All users should ensure that they have the latest edition of this publication.
7) No liability shall attach to IEC or its directors, employees, servants or agents including individual experts and members of its technical committees and IEC National Committees for any personal injury, property damage or other damage of any nature whatsoever, whether direct or indirect, or for costs (including legal fees) and expenses arising out of the publication, use of, or reliance upon, this IEC Publication or any other IEC Publications.
8) Attention is drawn to the Normative references cited in this publication. Use of the referenced publications is indispensable for the correct application of this publication.

The main task of IEC technical committees is to prepare International Standards. However, a technical committee may propose the publication of a technical report when it has collected data of a different kind from that which is normally published as an International Standard, for example "state of the art".

IEC TR 61282-13, which is a technical report, has been prepared by subcommittee 86C: Fibre optic systems and active devices, of IEC technical committee 86: Fibre optics.

The text of this technical report is based on the following documents:

Enquiry draft	Report on voting
86C/1201/DTR	86C/1236/RVC

Full information on the voting for the approval of this technical report can be found in the report on voting indicated in the above table.

This publication has been drafted in accordance with the ISO/IEC Directives, Part 2.

A list of all parts in the IEC 61280 series, published under the general title *Fibre-optic communication subsystem test procedures*, can be found on the IEC website.

The committee has decided that the contents of this publication will remain unchanged until the stability date indicated on the IEC web site under "http://webstore.iec.ch" in the data related to the specific publication. At this date, the publication will be

- reconfirmed,
- withdrawn,
- replaced by a revised edition, or
- amended.

A bilingual version of this publication may be issued at a later date.

INTRODUCTION

The International Electrotechnical Commission (IEC) draws attention to the fact that it is claimed that compliance with this document may involve the use of a patent concerning optical frequency-sensitive analyser given in 5.1.3.4 and concerning CD measurement using multi-tone probe signal given in 6.1.

IEC takes no position concerning the evidence, validity and scope of this patent right.

The holder of this patent right has assured the IEC that he/she is willing to negotiate licences either free of charge or under reasonable and non-discriminatory terms and conditions with applicants throughout the world. In this respect, the statement of the holder of this patent right is registered with IEC. Information may be obtained from:

Exfo Electro-Optical Engineering Inc.
400 Avenue Grodin
QC G1M 2K2
CANADA

JDS Uniphase Corporation
430 N. McCarthy Blvd.
Milpitas, CA 95035
USA

Attention is drawn to the possibility that some of the elements of this document may be the subject of patent rights other than those identified above. IEC shall not be held responsible for identifying any or all such patent rights.

ISO (www.iso.org/patents) and IEC (http://patents.iec.ch) maintain on-line data bases of patents relevant to their standards. Users are encouraged to consult the data bases for the most up to date information concerning patents.

FIBRE OPTIC COMMUNICATION SYSTEM DESIGN GUIDES –

Part 13: Guidance on in-service PMD and CD characterization of fibre optic links

1 Scope

This part of IEC 61282, which is a technical report, presents general information about in-service measurements of polarization mode dispersion (PMD) and chromatic dispersion (CD) in fibre optic links. It describes the background and need for these measurements, the various methods and techniques developed thus far, and their possible implementations for practical applications.

2 Normative references

The following documents, in whole or in part, are normatively referenced in this document and are indispensable for its application. For dated references, only the edition cited applies. For undated references, the latest edition of the referenced document (including any amendments) applies.

IEC 60793-1-42, *Optical fibres – Part 1-42: Measurement methods and test procedures – Chromatic dispersion*

IEC 61280-4-4, *Fibre optic communication subsystem test procedures – Part 4-4: Cable plants and links– Polarization mode dispersion measurement for installed links*

3 Symbols, acronyms and abbreviated terms

$D(\lambda)$	group velocity dispersion coefficient at optical wavelength λ
F	frequency of amplitude modulation in CD measurement
L	length of arc of the SOP rotation on the Poincaré sphere
L_f	length of fibre or fibre link
P_p, P_s	optical signal powers in two orthogonal SOPs
$\widehat{P}$	normalized optical power
$\Delta\widehat{P}$	normalized optical power difference
S_1 , S_2 , S_3	Stokes parameter
$\hat{S}$	normalized Stokes vector
N	number of statistically independent effective DGD measurements
N_t	number of statistically independent effective DGD measurements in time
N_v	number of statistically independent signal wavelengths
c	speed of light in vacuum
Δf	optical frequency interval or spacing
f	electrical signal frequency in dual-wavelength frequency generator
f_{clock}	clock frequency of digital data modulation
Δt	time interval between effective DGD measurements or differential time delay in CD measurement

Δt_{corr}	correlation time of effective DGD variations
$\Delta\phi$	differential phase shift in CD measurement
$\delta\lambda$	wavelength increment (interval, spacing or step size)
$\delta\nu$	optical frequency increment (interval, spacing or step size)
$\Delta\lambda$	optical source spectral width or linewidth (FWHM unless noted otherwise)
$\Delta\nu$	optical frequency interval or spacing
$\Delta\tau$	differential group delay value
$\Delta\tau_{eff}$	effective or partial DGD value, $\Delta\tau_{eff} = \Delta\tau \sin\varphi$, where φ is the angle between PSP vector and signal SOP vector on the Poincaré sphere
$<\Delta\tau>$	average DGD over a wavelength range or time interval
$<\Delta\tau_{eff}>$	average effective DGD over a wavelength range or time interval
$<\Delta\tau^2>^{1/2}$	average RMS DGD over a wavelength range or time interval
λ	optical wavelength
ν	optical light frequency
φ	angle between PSP and signal SOP vector on the Poincaré sphere
$\Phi(\nu)$	optical phase shift introduced by GVD in the spectral components of a modulated signal
ψ	angle between two Stokes vectors
σ	standard deviation of DGD measurements
θ	polarization rotation angle on the Poincaré sphere
ACF	autocorrelation function
ADC	analogue-to-digital converter
AM	amplitude modulation
ASE	amplified stimulated emission (from optical amplifiers)
BPF	optical or electrical band-pass filter
CD	chromatic dispersion
CW	continuous wave
DGD	differential group delay
DMUX	wavelength division de-multiplexer
DOP	degree of polarization
DPSK	differential phase shift keying
DSP	digital signal processing or processor
GVD	group velocity dispersion
JME	Jones matrix eigenanalysis (PMD test method)
LO	local oscillator or local oscillator laser
MT	monitoring port or tap
MUX	wavelength division multiplexer
NRZ	non-return-to-zero modulation
OA	optical amplifier
OOK	on-off keying
OTDR	optical time-domain reflectometry
PDF	probability density function

PC	variable polarization controller
PBS	polarization beam splitter
PD	photo detector
PM	phase modulation
PMD	polarization mode dispersion
PSK	phase shift keying
PSP	principal SOP
QPSK	quadrature phase shift keying
ROADM	reconfigurable optical add-drop multiplexer
RF	radio frequency
RZ	return-to-zero modulation
SOP	state of polarization
WDM	wavelength division multiplexing or multiplexer

4 Background

Excessive chromatic or polarization mode dispersion in fibre optic links may severely impair the transmission of high-speed optical signals. It is therefore important to accurately characterize the end-to-end optical properties of a fibre link before it is put into service. CD or PMD in a fibre link may be characterized using any of the measurement methods described in international standards, such as IEC 60793-1-42 for CD measurements and IEC 61280-4-4 for PMD measurements. A common feature of these methods is that they require either broadband or broadly tuneable optical probe signals to be injected into one end of the link while the optical properties of the fibre are analysed at the other end (see Figure 1). Consequently, the fibre link cannot carry any traffic during the duration of the measurement and has to be taken out of service.

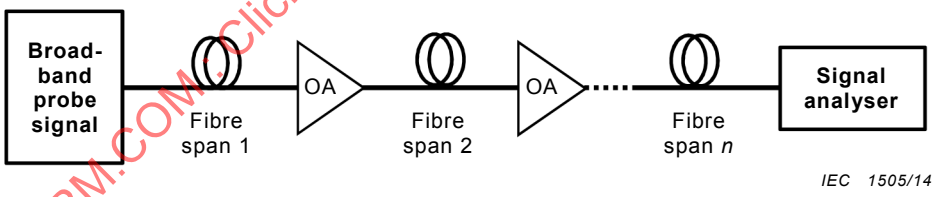

Key

OA optical amplifier

Figure 1 – Out-of-service fibre characterization with broadband optical probe signal

Such out-of-service measurements are usually acceptable when a new fibre link is installed. However, they are highly undesirable when the fibre dispersion needs to be re-measured in a link that already carries commercial traffic [1][1]. This situation may occur, for example, when a link is considered to be upgraded to a higher bit rate, e.g. from transmitting 10-Gb/s NRZ-OOK to 40-Gb/s DPSK signals, or during occasional troubleshooting. When conventional fibre characterization methods are used, all signals carried by the link have to be re-routed to other links before the measurement can be performed.

1 Numbers in square brackets refer to the Bibliography.

To avoid such time-consuming re-configuration of network traffic, various methods have been developed for measuring fibre properties in transmission links that carry live commercial traffic [2-11]. An important requirement for in-service fibre characterization is that the measurement procedure must not at any time interrupt or otherwise impair the transmission of traffic signals through the fibre.

This technical report describes the measurement principle and application of seven different in-service fibre characterization methods as well as their impact on network operation.

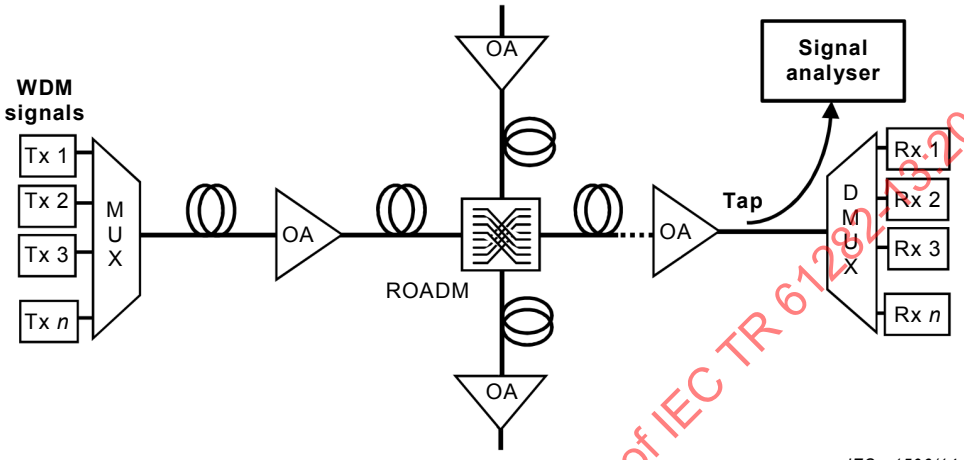

Key

Tx	optical transmitter
Rx	optical receiver
OA	optical amplifier
MUX	WDM multiplexer
DMUX	WDM demultiplexer
ROADM	reconfigurable optical add-drop multiplexer

Figure 2 – In-service fibre characterization with non-intrusive method

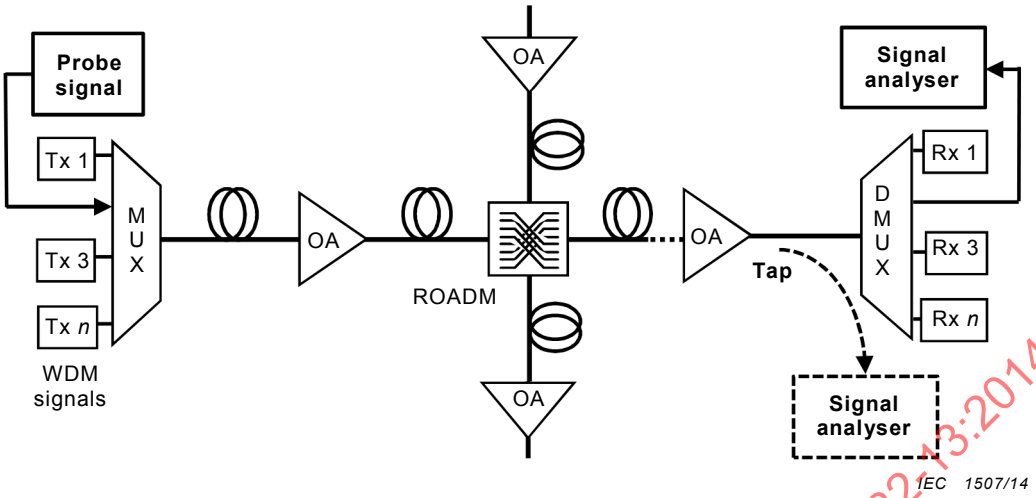

Key

Tx	optical transmitter
Rx	optical receiver
OA	optical amplifier
MUX	WDM multiplexer
DMUX	WDM demultiplexer
ROADM	reconfigurable optical add-drop multiplexer

Figure 3 – Semi-intrusive in-service fibre characterization using narrowband probe signal

In-service fibre characterization methods may be divided into three categories:

a) Completely non-intrusive methods which measure the desired fibre property by analysing the transmitted traffic signals at pre-installed monitoring ports (or taps) along the link, as shown in Figure 2. These methods do not interfere with the normal operation of the fibre link (just like in-service OSNR measurement techniques). Some of these methods employ high-speed optical receivers which recover or analyse the transmitted data [2-6], whereas others only analyse the spectral or polarization characteristics of the transmitted signal [7]. Non-intrusive methods have been employed to measure end-to-end CD and PMD.

b) Semi-intrusive methods which employ special optically narrow-band probe signals to measure the desired fibre property [8-12]. These probe signals are usually injected into unused (i.e. empty) WDM channels at the input of the link, via a pre-installed WDM multiplexer, and co-transmitted with the normal traffic signals, as shown in Figure 3. Methods using probe signals are generally considered to be intrusive, even though the measurement may not interrupt transmission of the traffic signals, because modern networks often require provisioning of the transport system to allow alien signals to pass through optical amplifiers and ROADM nodes. In addition, the co-transmission of probe signals may adversely affect the quality of the traffic signals through nonlinear interactions in the fibre (such as four-wave mixing or cross-phase modulation). Probe signals are often employed to measure end-to-end CD and PMD in fibre links and can be designed to be particularly sensitive to the fibre property to be measured [8, 10, 12]. However, the signals must meet the required optical power levels and/or spectral shape expected by optical channel monitors in ROADM nodes, as they otherwise may be blocked [1].

c) Out-of-band measurement methods using probe signals at optical frequencies that are outside of the band used for transmission of traffic signals. Pre-installed WDM couplers are required to inject and extract the probe signals without traffic interruption. Usually, out-of-band signals do not pass through optical amplifiers and/or ROADM nodes along the link. This method is predominantly used for in-service OTDR measurements to monitor fibre and connector losses during operation.

The non-intrusive fibre characterization methods of category a) avoid any interference with the network operation and, hence, may be performed at any time and over any desired length of time. This aspect is important if the fibre property to be measured fluctuates with time, like in the case of PMD, and needs to be monitored over a longer period of time [13]. Furthermore, all non-intrusive methods are single-ended measurements and, hence, require test equipment only at the receiving end of the fibre link, whereas the semi-intrusive methods of category b) need an additional probe signal generator at the input of the fibre link.

5 Non-intrusive fibre characterization

5.1 PMD measurement via polarization-sensitive spectral analysis

5.1.1 Introductory remark

This clause describes a truly non-intrusive method and apparatus for in-service PMD measurements on fibre links carrying conventional single-polarized WDM signals, i.e. signals that are transmitted in a single state of polarization (SOP). Just like many other out-of-service or intrusive PMD measurement methods, this method assumes that the PMD in the fibre link is composed of a large number of birefringent sections, which are randomly oriented and randomly distributed along the fibre link, so that the instantaneous DGD, measured at different optical frequencies and/or different times, is randomly distributed with a Maxwellian probability density function (PDF) [14].

It should be noted that the assumption of a Maxwellian PDF for the statistical distribution of the DGD is widely used to assess the PMD-induced transmission impairments of a fibre link. In fact, the main reason for measuring the mean DGD in fibre links is to estimate the probability of PMD-induced transmission outages, which can occur when the randomly varying DGD exceeds a certain maximal value, beyond which the transmitted signals may become severely distorted, so that they cannot be received without errors [14].

The likelihood of transmission outages in a fibre link can be determined from the measured value of the mean DGD only if the statistical distribution of the DGD is known. This distribution is normally assumed to have a Maxwellian PDF, and this assumption has been preponderantly confirmed in numerous investigations of medium- and long-distance fibre links. Therefore, the assumption of a Maxwellian-distributed DGD in the method described below does not restrict its applicability for measuring the mean DGD in fibre links to assess the likelihood of PMD-induced transmission outages.

The method employs a combined optical spectrum and polarization analyser, i.e. a spectrally narrowband polarimeter whose centre frequency can be tuned continuously over a sufficiently large range. This analyser is connected to a broadband monitoring port at the end of a fibre link and measures the optical frequency dependence of the polarization state in each transmitted optical signal. The optical resolution bandwidth of this analyser has to be substantially smaller than the spectral bandwidth of each data-carrying signal transmitted over the fibre link. This polarization-sensitive spectral analysis may be performed on any single-polarized signal, having arbitrary launch SOP, and does not require knowledge of the particular modulation format or symbol rate of the transmitted signals. Thus, it may be readily applied in mixed transmission systems carrying signals of different symbol rates and/or modulation formats.

The polarization analysis shall be performed – either simultaneously or consecutively – on all WDM signals that traverse the fibre link under test, but shall not include polarization-multiplexed signals or signals that have traversed other fibre links prior to entering the selected link. From this set of measurements one can then estimate the mean DGD in the fibre link, as explained in more detail in 5.1.2. Just like for conventional PMD measurements, the uncertainty of this estimate depends on the frequency range covered by the analysed WDM signals, as well as on the number of WDM signals included in the set of measurements. In general, the uncertainty is smallest when the WDM signals are equidistantly distributed over the largest possible frequency range (see 5.1.4 for more details).

The uncertainty of the estimated mean DGD may be reduced further by repeating the polarization analysis on the transmitted WDM signals periodically over a sufficiently long time interval. The mean DGD in the fibre link is then determined from the time- and frequency-average of the measured frequency dependence of the polarization state variations in the individual signal spectra. In the extreme case, the mean DGD in a fibre link may be assessed from a set of periodically repeated polarization analyses on just one selected WDM signal. The uncertainty of the mean DGD derived from these single-signal measurements depends on the total measurement time and may be estimated from the speed and magnitude of the DGD fluctuations observed in the measurements (see 5.1.4).

Therefore, this method may be applied to directly measure the end-to-end PMD of individual signal paths in ROADM networks, wherein the various WDM signals may traverse different fibre spans, because they are added (and dropped) at different locations. As a result, one may find fibre links where only a small number of the received signals have traversed the exact same signal path. Only these signals should be included in the polarization analysis and used to calculate the mean DGD. Because the uncertainty of a PMD measurement generally increases inversely with the number of analysed signals, it is important to include all signals in the analysis that have traversed the same signal path. The benefits of using more signals is limited by their correlations, as explained in more detail in 5.1.4.

End-to-end PMD measurements of signal paths generally avoid errors associated with the concatenation of span-by-span PMD characterization. Furthermore, because the PMD analysis may be performed at other points along the fibre link where a monitoring tap is installed, it may thus be possible to identify fibre sections with particularly high PMD values. In either case, performing these in-service PMD measurements has absolutely no impact on the operation of the network. The accuracy of the method has been asserted in lab experiments as well as in field trials and found to be within a few per cent of that of standard methods over a wide range of DGD values [6-7].

5.1.2 Measurement principle

End-to-end PMD in a fibre link may be characterized by the mean DGD, $<\Delta\tau>$, or alternatively by the RMS DGD, $<\Delta\tau^2>^{1/2}$, which is closely related to $<\Delta\tau>$. For example, $<\Delta\tau>$ can be readily determined by measuring the DGD, $\Delta\tau$, at various optical frequencies across the transmission band and averaging the results (see also IEC 61280-4-4). However, $<\Delta\tau>$ may also be obtained by averaging a set of $\Delta\tau$ measurements which are taken at the same optical frequency and repeated several times over a sufficiently long time interval, or from the average of a set of $\Delta\tau$ measurements taken at different times and frequencies [6, 14]. In either case, such DGD measurements typically require a special probe signal as well as knowledge or even control of the launch polarization state of the probe signal, whereas commercial WDM signals are usually launched with arbitrary polarization states which may not be controlled, varied or aligned.

The PMD-induced waveform distortion or pulse spreading in a WDM signal with arbitrary launch SOP depends on the orientation of the launch SOP relative to the usually unknown and randomly oriented input principal state of polarization (PSP) of the fibre at the signal wavelength. It may be characterized by a parameter commonly referred to as “effective” or “partial” DGD, $\Delta\tau_{eff}$ This quantity is defined as the magnitude of the component of the PMD vector in Stokes space that is orthogonal to the launch polarization state of the optical signal [6, 15]. Its relation to the instantaneous DGD $\Delta\tau$ is

$$\Delta\tau_{eff} = \Delta\tau \sin\varphi \tag{1}$$

wherein φ denotes the aforementioned angle between the Stokes vectors representing the launch SOP of the signal and the input PSP of the fibre.

It is easily seen that $\Delta\tau_{eff} = \Delta\tau$ if the launch SOP is an equal mix of the two input PSPs, and $\Delta\tau_{eff} = 0$ if the launch SOP is identical with one of the two PSPs. For fibre links having

preponderantly randomly distributed and oriented birefringence, the statistical distribution of $\Delta\tau$, measured at different optical frequencies and/or at different times, is described by a Maxwellian PDF, whereas the PSPs are randomly oriented in Stokes space [14]. Consequently, the statistical distribution of the angle φ in Equation (1) is uniform (e.g. in the interval between 0 and π), even when the various WDM signals are launched in random, mutually different polarization states, and the corresponding statistical distribution of $\Delta\tau_{eff}$ is given by a Rayleigh PDF [6, 14, 15],

$$\frac{\Delta\tau_{eff}}{<\Delta\tau^2>}\ \exp\left(-\frac{\Delta\tau_{eff}{}^2}{2<\Delta\tau^2>}\right) \tag{2}$$

which depends only on the parameter $<\Delta\tau^2>$, just like the Maxwellian PDF for $\Delta\tau$, even though the two distributions are substantially different, as shown in Figure 4.

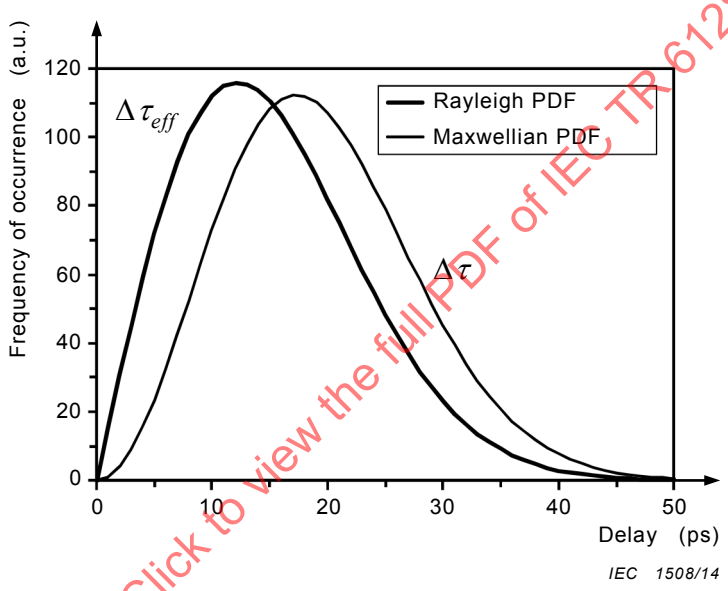

Figure 4 – Rayleigh PDF for $\Delta\tau_{eff}$ compared with Maxwellian PDF for $\Delta\tau$

Since both statistical distributions depend only on the parameter $<\Delta\tau^2>$, it is therefore possible to deduce the mean DGD $<\Delta\tau>$ from the mean effective DGD $<\Delta\tau_{eff}>$, which may be determined from a sufficiently large statistical ensemble of $\Delta\tau_{eff}$, measurements, as explained in more detail in 5.1.3 and 5.1.4. In fact, the mean DGD $<\Delta\tau>$ is directly proportional to the mean value $<\Delta\tau_{eff}>$ [6, 14, 15], i.e.

$$<\Delta\tau> = (4/\pi)<\Delta\tau_{eff}> \tag{3}$$

Thus, the mean DGD in a fibre link may be determined from a set of in-service measurements of $\Delta\tau_{eff}$ on the transmitted optical signals. These measurements do not require knowledge or control of the launch SOPs of the analysed signals and, hence, are truly non-intrusive. In fact, the launch SOPs can be all identical, and therefore highly correlated, or completely random and mutually uncorrelated. The statistical distribution of φ and hence $\Delta\tau_{eff}$ in Equation (1) is the same in either case, because of the random orientation of the PSPs at the various signal frequencies.

To minimize the measurement uncertainty of the mean value $<\Delta\tau_{eff}>$, the polarization analysis should be performed, either simultaneously or consecutively, on all WDM signals that

traverse the link under test, but should not include signals that have traversed other fibre links prior to entering the link under test. If the number of analysed signals is small and/or if their frequencies are not spaced sufficiently far apart (see 5.1.4.2), the $\Delta\tau_{eff}$ measurements shall be repeated several times at predetermined time intervals Δt over a sufficiently long time period, which in some cases, may be several hours or even several days, depending on the speed and magnitude of the PMD fluctuations in the fibre link. A more detailed discussion of the measurement accuracy is provided in 5.1.4.

5.1.3 Methods for measuring $\Delta\tau_{eff}$ via polarization analysis

5.1.3.1 Introductory remark

In general, PMD introduces frequency-dependent variations in the SOP of a polarized optical signal, so that the various spectral components of a modulated optical signal passing through the fibre link are transformed into different SOPs. Within a sufficiently narrow optical bandwidth $\Delta\nu$ (typically less than $0{,}16/\langle\Delta\tau\rangle$), the frequency-dependent polarization transformations may be approximated by a uniform rotation about a fixed axis on the Poincaré sphere, as shown schematically in Figure 5.

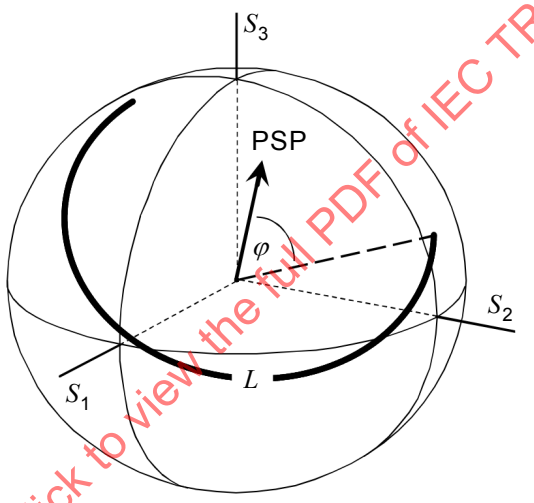

Key

S_1, S_2, S_3	Stokes parameter
L	length of polarization rotation trace
φ	angle between PSP and signal SOP

Figure 5 – PMD-induced polarization rotation within the spectrum of a modulated signal

The rotation axis is defined by the orientation of the PSPs, while the rotation rate is proportional to $\Delta\tau$. For a signal with optical bandwidth $\Delta\nu$, the full rotation angle is given by $\Phi = 2\pi\,\Delta\tau\,\Delta\nu$, whereas the length, L, of the arc traced by the SOP rotation is $L = 2\pi\,\Delta\tau_{eff}\,\Delta\nu$.

5.1.3.2 Frequency-selective polarimeter

A general method for measuring $\Delta\tau_{eff}$ in a modulated optical signal is to analyse the frequency-dependent SOP variations across the spectrum of the signal. This can be accomplished, for example, with the help of a narrowband, frequency-tuneable optical polarimeter, like the apparatus shown schematically in Figure 6 [15]. With this instrument, it may even be possible to directly determine $\Delta\tau$ from the Poincaré sphere analysis. However, such measurements of the actual DGD become very unreliable when the launch SOP is nearly identical with one of the two PSPs of the fibre at the centre wavelength of the signal (see 5.3.3.2 below).

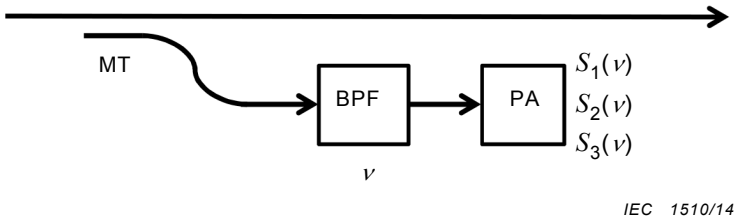

Key

MT monitoring tap

BPF tuneable band-pass filter

PA complete polarization analyser (polarimeter)

Figure 6 – Set-up for measuring PMD-induced polarization rotations in optical signals

5.1.3.3 Frequency- and polarization-selective analyser

An alternative method and apparatus for measuring $\Delta\tau_{eff}$ is shown in Figure 7. It employs a simple polarization splitter in combination with a variable polarization transformer and a tuneable optical band-pass filter to analyse the SOP variations in the signal spectrum. The advantage of this apparatus is that it is significantly easier to calibrate than the full polarimeter of Figure 6. The function of the polarization transformer in Figure 7 is to adjust the relative orientation of the PMD-induced polarization rotation so that

a) the SOP at the centre of the signal spectrum ($\nu=0$) is a 50/50 mix of the two eigenstates of the polarization splitter, and

b) the axis of the PMD-induced rotation (on the Poincaré sphere) is orthogonal to the eigenstates of the PBS.

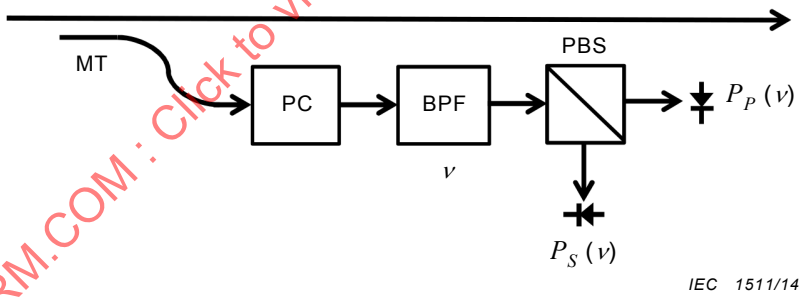

Key

MT monitoring tap

BPF tuneable band-pass filter

PC variable polarization controller

PBS polarization beam splitter

Figure 7 – Modified set-up for measuring PMD-induced polarization rotations

The transformation described above yields the highest sensitivity of the detector signals, P_p and P_s, to the PMD-induced polarization rotation and, hence, may be found by scanning the tuneable filter repeatedly across the signal spectrum at different settings of the input polarization transformer, until a scan is found wherein $P_p \approx P_s$ and $\left|\partial P_p/\partial\nu\right| = \left|\partial P_s/\partial\nu\right|$ is maximal at $\nu=0$ [6]. Once the desired transformation is obtained, $\Delta\tau_{eff}$ may be calculated, in a straightforward manner, from the frequency dependence of the rotation angle [7]

$$\theta(\nu) = 2\arctan\left(\sqrt{\frac{P_{\mathrm{p}}(\nu)}{P_{\mathrm{s}}(\nu)}}\right) \tag{4}$$

yielding a single value for $\Delta\tau_{eff}$ for each WDM signal

$$\Delta\tau_{eff} = \left|\frac{\partial\theta(\nu)}{2\pi\,\partial\nu}\right| \tag{5}$$

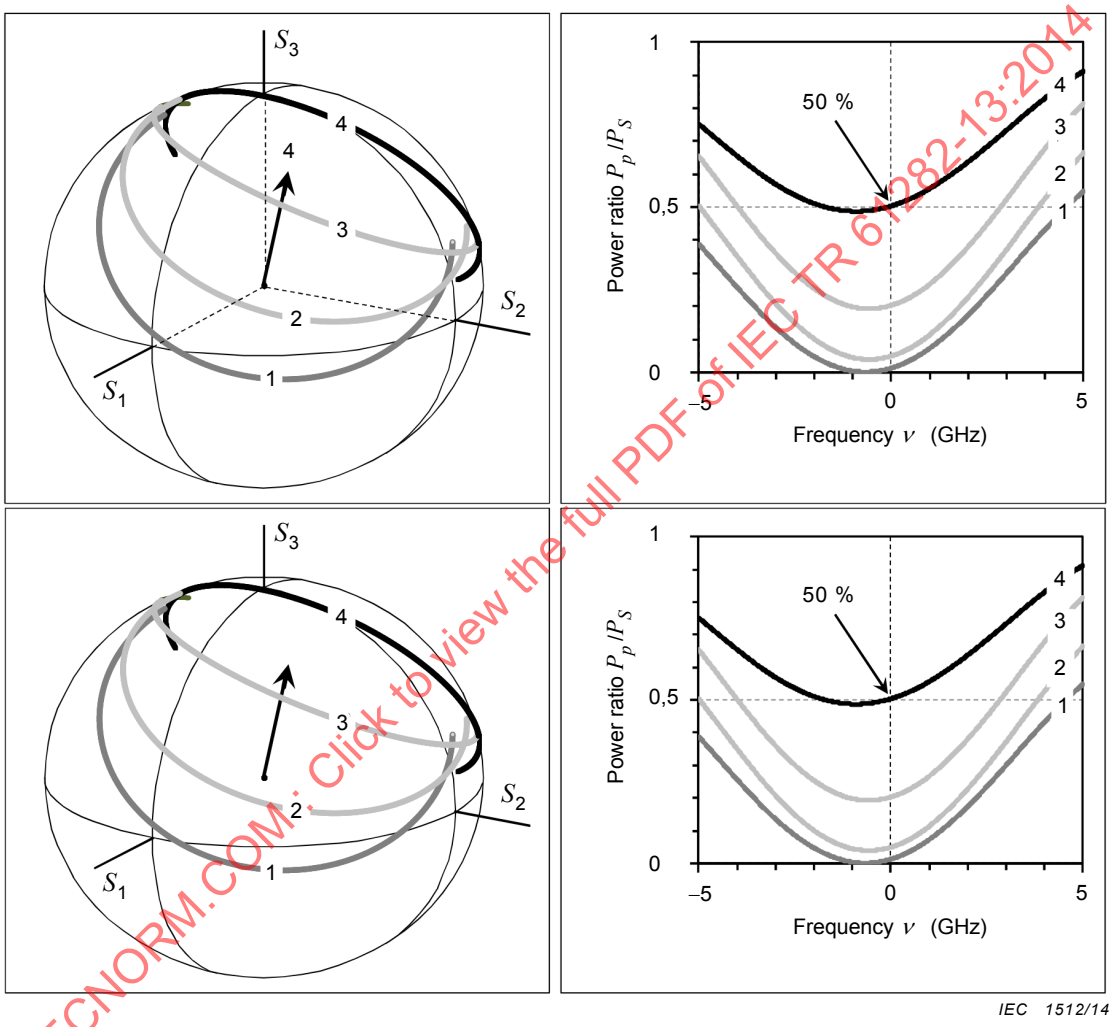

Figure 8 – Sequence of polarization transformations leading to a scan with $P_{\mathrm{p}} \approx P_{\mathrm{s}}$ at ν=0 (left) and corresponding power ratios (right)

The procedure to obtain the desired polarization transformation is demonstrated in Figure 8 and 9 below. Figure 8 displays a series of polarization transformations on the Poincaré sphere, starting with the initial scan of Figure 5 and ending with a scan wherein $P_{\mathrm{p}} \approx P_{\mathrm{s}}$ at $\nu = 0$ but $\left|\partial P_{\mathrm{p}}/\partial\nu\right|$ is not yet maximized. The eigenstates of the polarization splitter are assumed to be at S_1 = ±1. Furthermore, Figure 9 displays a set of transformations with $P_{\mathrm{p}} \approx P_{\mathrm{s}}$ but different slopes of the rotation angle $\theta(\nu)$. The desired final transformation is the one in which $\left|\partial\theta/\partial\nu\right|$ is maximal.

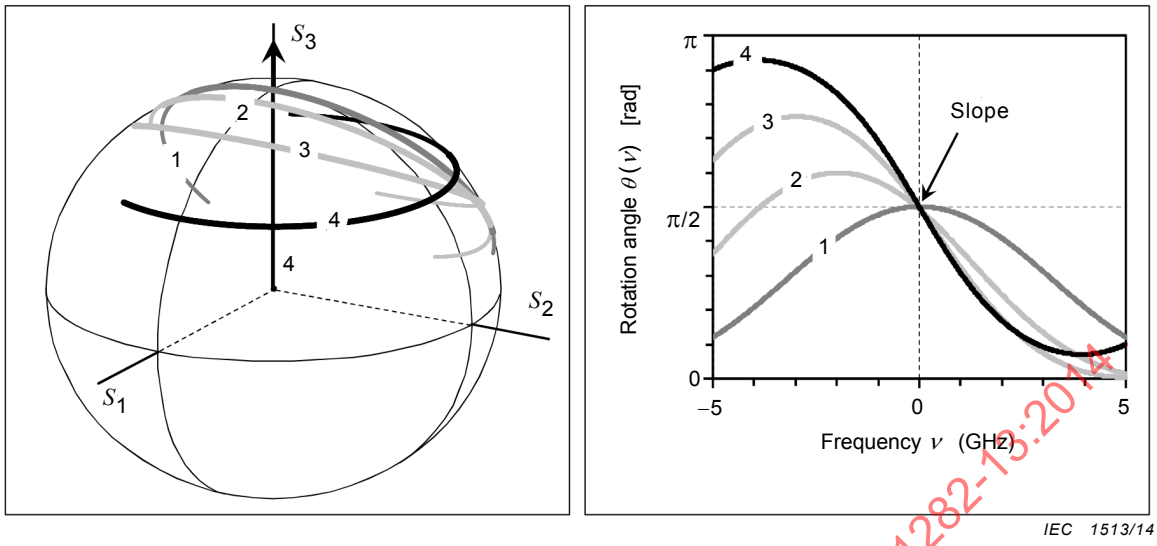

Figure 9 – Sequence of polarization transformations with $P_p \approx P_s$ at ν=0 (left) and corresponding rotation angles (right)

5.1.3.4 Optical frequency-selective analyser with polarization scrambling

Another useful method for measuring $\Delta\tau_{eff}$ with the apparatus of Figure 7 is to operate the polarization controller as a random polarization scrambler and analyse – for each setting of the polarization scrambler – the differences in optical intensity at two closely spaced optical frequencies within the spectral width of the analysed signal. Close examination of the polarization traces on the Poincaré sphere in Figures 8 and 9 reveals that the shape of arc resulting from the PMD-induced, frequency-dependent polarization transformations within the signal spectrum is independent of the settings of the polarization controller. Therefore, the distance between any two normalized Stokes vectors describing the PMD-induced arc at optical frequencies ν_1 and ν_2 remains always the same. In other words, if $\hat{S}(\nu_1)$ and $\hat{S}(\nu_2)$ are the two Stokes vectors, then

$$\left|\hat{S}(\nu_1)-\hat{S}(\nu_2)\right| = \sqrt{2-2\cos\psi} = \sqrt{2}\,\sin(\psi/2) \tag{6}$$

is independent of the settings of the polarization controller, because its linear polarization transformations do not affect the angle between these two Stokes vectors, ψ, which is given by

$$\psi = \Phi\,\sin\varphi = 2\pi\,\Delta\tau_{eff}\left|\nu_1-\nu_2\right|. \tag{7}$$

The magnitude of ψ is then determined from a set of measurements of the normalized optical power of the two polarization-analysed signals at frequencies ν_1 and ν_2, i.e. from $\hat{P}(\nu_1)=P_p(\nu_1)/\left[P_p(\nu_1)+P_s(\nu_1)\right]$ and $\hat{P}(\nu_2)=P_p(\nu_2)/\left[P_p(\nu_2)+P_s(\nu_2)\right]$, which are taken at various settings of the polarization controller. As clearly seen in the right-most graphs in Figures 8 and 9, the optical power of the polarization-analysed signals exiting the polarization splitter depends very sensitively on the polarization transformation introduced by the polarization controller, because $\hat{P}(\nu)=\left|1+\hat{S}(\nu)\bullet\hat{S}_a\right|/2$, where $\hat{S}_a$ denotes the Stokes vector of the eigenstate of the polarization splitter. However, if the polarization controller scrambles the polarization state of the received signal in such a way that the polarization states seen by the polarization splitter, on average, are approximately uniformly distributed on the Poincaré sphere, so that

$$\left\langle S_i^2(\nu)\right\rangle_{SOP} = 1/3 \tag{8}$$

then the root-mean-square value of the normalized power difference $\Delta\hat{P} = \hat{P}(\nu_1) - \hat{P}(\nu_2)$ becomes proportional to Equation (6). The brackets $<...>_{SOP}$ in Equation (8) indicate averaging over all settings of the polarization controller and S_i are the components of the normalized Stokes vector $\hat{S}(\nu)$, with i = 1 ... 3. After straightforward calculations one then finds

$$\Delta\tau_{eff}(\nu) = \frac{\arcsin\left[\sqrt{3\left\langle\Delta\hat{P}^2(\nu)\right\rangle_{SOP}}\right]}{\pi\,|\nu_1 - \nu_2|} \tag{9}$$

where $\nu = (\nu_1+\nu_2)/2$.

Equation (9) may be evaluated at arbitrary frequencies ν_1 and ν_2 within the spectral width of the analysed signal. In particular, it may be evaluated for a multitude of different frequency pairs. However, the frequency separation $\Delta\nu = |\nu_1-\nu_2|$ of any of these pairs should not exceed $0{,}5/\Delta\tau_{eff}$ as Equation (9) otherwise produces erroneous results. In cases where the mean DGD and the frequency spacing $\Delta\nu = |\nu_1-\nu_2|$ both are large, the value calculated from Equation (9) may not be representative of the actual effective DGD at the centre frequency of the WDM channel but rather an average of $\Delta\tau_{eff}$ at the two analysed frequencies. However, such partial averaging should not have a significant impact on the accuracy of the average DGD calculated from Equation (3).

5.1.4 Measurement accuracy

5.1.4.1 Individual $\Delta\tau_{eff}$ measurements

The accuracy of a measurement of $\Delta\tau_{eff}$ depends not only on the particular implementation of the measurement equipment (e.g. the accuracy and dynamic range of the polarization analyser), but also on the spectral width of the analysed signals and the resolution bandwidth of the instrument. As a general rule of thumb, it may be assumed that the minimal spectral bandwidth of a modulated signal, over which $\Delta\tau_{eff}$ can be measured, is approximately equal to its symbol rate expressed in Hz. For example, the SOP of conventional 2,5 GBd and 10 GBd NRZ-OOK signals may be analysed over a frequency range of ±1,25 GHz and ±5 GHz around the carrier frequency, respectively, whereas that of a 40 GBd NRZ-DPSK signal may be analysed over a total frequency range of ±20 GHz.

Hence, when a 10 GBd NRZ-OOK signal experiences DGD of 1 ps, the useful length L in Figure 5 is about 0,064, or 1 % of a full great circle. To accurately measure the length of such a short arc requires a tuneable filter with high spectral resolution and precise frequency calibration. For the measurement method described above in 5.1.3.3, the spectral resolution of the polarization analyser should be better than about 20 % of the useful spectral range, i.e. about 500 MHz in the case of a 2,5 GBd signal and 2 GHz for a 10 GBd signal. On the other hand, high spectral resolution is also required when measuring $\Delta\tau_{eff}$ in signals that have experienced large amounts of DGD. In the method described in 5.1.3.3, the rotation angle $\theta(\nu)$ may become a very steep function of optical frequency. With a DGD of 100 ps, for example, the slope of $\theta(\nu)$ may be up to 3 times steeper than the steepest slope displayed in Figure 9, thus requiring sub-GHz frequency resolution for accurate measurement of $\Delta\tau_{eff}$.

For the method described in 5.1.3.4, the frequency separation $\Delta\nu$ should be as large as possible when measuring small DGDs, so as to increase the accuracy of the measurement, but should not exceed $0{,}5/\Delta\tau_{eff}$, as explained above. In general, the accuracy of the measurement increases with the number of frequency pairs included in the analysis. The spectral resolution of the band-pass filter before the polarization analyser can be significantly

larger than that required for the method in 5.1.3.3. Under certain conditions, the measurements may be performed with a polarization scrambler followed by a polarization-diverse optical spectrum analyser having relatively moderate spectral resolution of up to 40 % of the useful spectral range. However, increasing the spectral resolution of the analyser to such large values may result in frequency-averaged measurements of $\Delta\tau_{eff}$.

The measurement accuracy may also be impacted by large polarization fluctuations in the fibre, caused, for example, by mechanical movement of the fibre. Polarization rotations at rates of up to 1 000 rad/s have been observed [16]. Since these rotations are superimposed on the PMD-induced polarization rotation, they can potentially cause large measurement errors. To minimize these errors, the tuneable filter in Figure 7 should be scanned at the highest possible speed across each signal spectrum. Consider, for example, a filter that scans in 1 ms across a 100 GHz wide signal channel. Even at this high tuning rate, the aforementioned polarization fluctuations of 1 000 rad/s would introduce a small measurement error of up to 1,6 ps in $\Delta\tau_{eff}$. However, the measurement errors caused by polarization fluctuations tend to be random and not systematic. Therefore, as long as they are sufficiently small, these errors effectively cancel one another when calculating $<\Delta\tau_{eff}>$ from a large set of individual $\Delta\tau_{eff}$ measurements.

Systematic measurement errors, on the other hand, need to be kept very small, because they add linearly to $<\Delta\tau_{eff}>$.

5.1.4.2 Mean value of $\Delta\tau_{eff}$

Aside from the measurement errors in $\Delta\tau_{eff}$ discussed above, the accuracy of $<\Delta\tau_{eff}>$ also depends strongly on the total number of measurements performed at different frequencies and/or different times on the optical signals. Because $\Delta\tau_{eff}$ is a statistical variable, which varies randomly with time and frequency, the uncertainty in estimating $<\Delta\tau_{eff}>$ from a set of measurements may be characterized by the standard deviation of the Rayleigh PDF [13, 14, 17],

$$\sigma = 0{,}523 <\Delta\tau_{eff}> \Big/ \sqrt{N} \tag{10}$$

wherein N denotes the total number of statistically independent samples in the ensemble of $\Delta\tau_{eff}$ measurements.

Measurements that are performed simultaneously (or consecutively at nearly the same time) on two signals with different carrier frequencies, ν_1 and ν_2, are considered to be statistically independent when the frequency spacing, $\Delta\nu = |\nu_1 - \nu_2|$, is substantially larger than $0{,}5/<\Delta\tau>$ [14, 17]. If the signals are spaced at least 50 GHz apart, for instance, the $\Delta\tau_{eff}$ measurements are statistically independent when $<\Delta\tau>$ is larger than 10 ps.

Likewise, measurements taken at two different times, t_1 and t_2, on the same optical signal are considered statistically independent when time interval, $\Delta t = |t_1 - t_2|$, is substantially larger than the correlation time, Δt_{corr}, of the time-varying PMD fluctuations in the fibre link. Since PMD fluctuations generally arise from changes in the physical environment of the fibre (e.g. temperature variations), which may be very different in different links, Δt_{corr} may vary widely from link to link and, therefore, is usually unknown prior to a PMD measurement.

Thus, to assess the accuracy of $<\Delta\tau_{eff}>$, it may be necessary to estimate Δt_{corr} from a series of time-consecutive measurements by calculating, separately for each signal frequency, the normalized autocorrelation function [13],

$$ACF(\Delta t\,;\nu) = C \int_0^T \left[\Delta\tau_{eff}(t\,,\nu) - <\Delta\tau_{eff}>\right] \times \left[\Delta\tau_{eff}(t+\Delta t,\nu) - <\Delta\tau_{eff}>\right] dt \tag{11}$$

where T denotes the total measurement time and C is a suitable normalization constant. The mean correlation time Δt_{corr} may then be determined from the averaged auto-correlation function $ACF(\Delta t) = < ACF(\Delta t\,;\nu) >_{\nu}$, where the average is taken over all optical frequencies. When $\Delta\tau_{eff}$ is measured repeatedly over a sufficiently long time interval T, $ACF(\Delta t)$ decreases monotonically with Δt, so that Δt_{corr} may be obtained as the time when $ACF(\Delta t)$ has decreased to $1/e$ of its value at t=0, i.e. $ACF(\Delta t_{corr}) = ACF(0)/e$.

Once Δt_{corr} is known, the expected measurement uncertainty in $<\Delta\tau_{eff}>$ may be estimated from the standard deviation in Equation (10) by using $N = N_t \times N_\nu$, wherein $N_t \leq T/t_{corr}$ is the number of statistically independent measurements in time and N_ν the number of statistically independent signal frequencies ν.

5.1.5 Measurement set-up example

5.1.5.1 Apparatus for measuring $\Delta\tau_{eff}$

An exemplary implementation of an apparatus suited to measure $\Delta\tau_{eff}$ in a WDM network is shown schematically in Figure 10. This apparatus is based on the measurement principle shown in Figure 7, but employs a tuneable coherent detector with polarization diversity to analyse the frequency dependence of the signal's SOP [6]. In this implementation, the signal component to be analysed is selected by the frequency of the tuneable local oscillator laser of the coherent detector, and the spectral resolution of the instrument is determined by the electrical bandwidth of the receiver circuit.

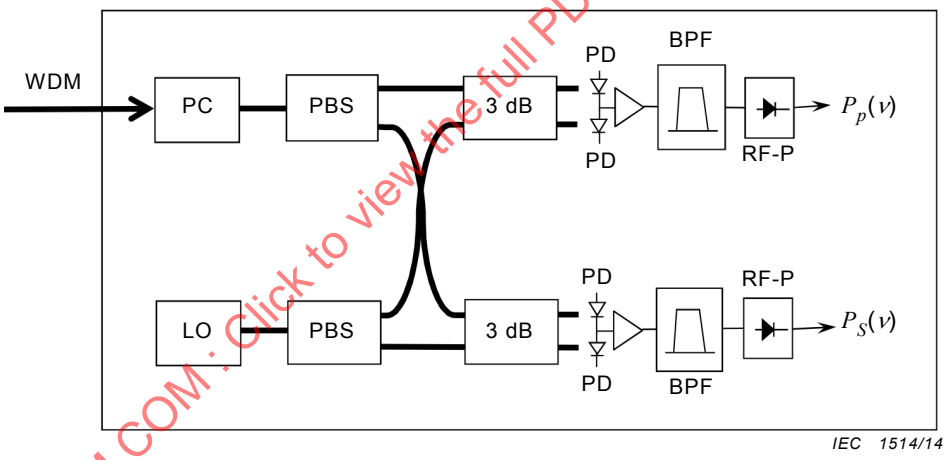

Key

PC	variable polarization controller
PBS	polarization beam splitter
3 dB	3-dB power splitter
PD	photo-detector
BPF	electrical band-pass filter
RF-P	RF power detector

Figure 10 – Apparatus using coherent detection to measure $\Delta\tau_{eff}$

Just like in the setup shown in Figure 7, the incoming optical signals first pass through a variable polarization controller before they are separated into two orthogonal polarization components by a polarization splitter. The two polarization components are then separately mixed with the output light of a tuneable local oscillator laser and the resulting beat signals are detected with two balanced photo-receivers. The received electrical signals are bandwidth limited (e.g. to about 200 MHz) before they are fed into two RF-power detectors, which generate two electrical signals, $P_p(\nu)$ and $P_s(\nu)$. These two signals are proportional to the

optical signal power in the two orthogonal SOPs within a narrow bandwidth around optical frequency ν. The spectral resolution of the instrument is about twice the bandwidth of the electrical band-pass filters in the receiver (e.g. about 400 MHz).

The two electrical signals, $P_p(\nu)$ and $P_s(\nu)$, are recorded and analysed while the local oscillator laser scans rapidly across the spectrum of the selected WDM signal (e.g. at a rate of 100 GHz/ms and with sub-GHz accuracy). This scan is repeated several times at various settings of the input polarization transformer so as to obtain the desired scan with $P_p \approx P_s$ and maximal slope $|\partial\theta/\partial\nu|$ at the centre frequency of the signal, using the procedure described in 5.1.3. As described in 5.1.4.1, it is important to scan the local oscillator laser at the fastest possible rate, so as to minimize measurement errors caused by polarization fluctuations in the analysed signal. A tuning rate of 100 GHz/ms is sufficient to ensure that even rapid SOP fluctuations of up to 1 000 rad/s introduce only negligible measurement errors.

The high-frequency selectivity of the coherent receiver allows high-resolution spectral analysis of the transmitted signals and, hence, measurement of $\Delta\tau_{eff}$ over a wide range of DGD values. A comparison of PMD measurements taken with such a receiver on various combinations of single-mode fibres and PMD emulators, with $<\Delta\tau_{eff}>$ ranging from 1 ps to 50 ps, showed very good agreement with reference measurements taken with a commercial JME analyser [7]. The accuracy of in-service PMD measurements has also been evaluated in various field trials. Tests on a terrestrial fibre link with buried cables, for example, have shown that accurate PMD measurements can be obtained within a few hours of total measurement time [13].

5.1.5.2 Exemplary procedure for in-service PMD measurements

To analyse the PMD in a given fibre link, one may perform the following steps:

a) Connect PMD analyser to a broadband monitoring port at the end of the fibre link to be analysed.

b) Scan analyser over the entire transmission band to detect all signals arriving at receiver.

c) From these signals, select those suitable to be included in the PMD analysis (i.e. those that traverse the entire fibre link to be analysed).

d) Determine $\Delta\tau_{eff}$ from the frequency-selective polarization rotation in the selected signals .

e) Calculate the mean values $<\Delta\tau_{eff}>$ and $<\Delta\tau>$ from these measurements.

f) Calculate the number of statistically independent measurements in frequency and determine measurement uncertainty from Equation (10).

g) If measurement uncertainty is too large, repeat measurement of $\Delta\tau_{eff}$ on selected signals after a predetermined waiting period (e.g. 30 min).

h) Calculate average correlation time of $\Delta\tau_{eff}$ in each selected signal channel and determine number of statistically independent measurements in time.

i) Re-calculate measurement uncertainty from Equation (10).

j) Repeat steps g) through i) until measurement uncertainty is satisfactory.

5.2 CD and PMD measurements based on high-speed intensity detection

5.2.1 Introductory remark

This clause describes several methods for non-intrusive measurements (or monitoring) of chromatic dispersion (CD) and PMD in fibre optic links carrying commercial traffic. Similar to the DGD measurements described in 5.1, it is possible to measure the end-to-end group velocity dispersion (GVD) in a fibre link by analysing the properties of a transmitted WDM signal. GVD introduces frequency-dependent optical phase shifts in the various spectral components of the transmitted optical signal which, to first order, are proportional to the square of the optical frequency [18],

$$\Phi(\nu) = \pi\, \lambda^2\, \nu^2\, D(\lambda)\, L_f \,/ c \qquad (12)$$

where

$D(\lambda)$ denotes the GVD per unit length in the fibre (e.g. in units of ps/nm/km);

L_f is the the length of the fibre link,

ν is the optical frequency,

λ is the optical wavelength, and

c the speed of light.

Equation (12) ignores higher order CD, which is justified here because of the relatively narrow optical bandwidth of a single WDM signal. However, the frequency dependence of CD (i.e. the dispersion slope) may be determined by measuring GVD in several different WDM channels across the transmission band of interest. It should be noted that the CD-induced phase shifts $\Phi(\nu)$increase linearly with the accumulated GVD in the fibre link.

It is quite difficult to measure the CD-induced phase shifts of Equation (12) directly in the optical spectrum of the signal. However, they often can be measured indirectly by assessing the resulting pulse distortions with a high-speed intensity detector, as described below, or by mixing the signal with a local oscillator laser in a high-speed coherent receiver, as described in 5.3.2. In any case, detailed knowledge of the signal's modulation characteristics (e.g. modulation format, symbol rate, and rise- and fall-times) is required in order to distinguish the CD-induced phase shifts from those introduced by encoding the transmitted data.

The most basic technique to detect GVD (and DGD) in a modulated signal is to beat the spectral components of the entire signal simultaneously in a high-speed photo-detector and then analyse the resulting photo-current as a function of time, as shown in Figure 11. Alternatively, one may analyse the spectral composition of the photo-current in the frequency domain.

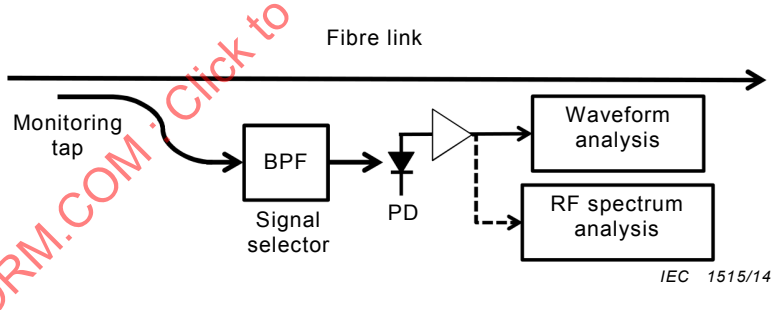

Key

BPF optical band-pass filter

PD high-speed photo-detector

Figure 11 – Apparatus for GVD measurements in a transmitted signal using a high-speed receiver with time-domain waveform analysis or, alternatively, RF spectrum analysis

In either case, a tuneable optical band-pass filter is needed to isolate the signal to be measured from other transmitted WDM signals. The measurement principle is based on the fact that the CD-induced phase shifts in the signal's spectrum cause partial conversion of amplitude modulation (AM) into phase modulation (PM), and conversely, PM into AM [19]. Because photo-detectors are only sensitive to AM (but not to PM), the CD-induced AM-PM conversion significantly alters the electrical waveforms of the received photo-current. These waveform distortions occur with conventional on-off keyed (OOK) signals as well as with advanced phase-shift keyed (PSK) signals and may either be measured in the time domain,

as described in 5.2.2, or as variations in the RF spectrum of the detector signal, as described in 5.2.3.

Most measurement methods based on waveform distortions cannot distinguish between positive and negative GVD, because the distortions usually do not depend on the sign of the accumulated GVD [6, 19]. However, it is possible to determine the sign of GVD by performing a second measurement with an additional CD element of known GVD inserted into the optical path, as shown schematically in Figure 12. If the second measurement yields higher GVD than the first one, the accumulated GVD in the fibre link has the same sign as the GVD of the reference element [20]. Conversely, if the GVD of the second measurement is lower than that of the first one, the GVD in the fibre link has the opposite sign.

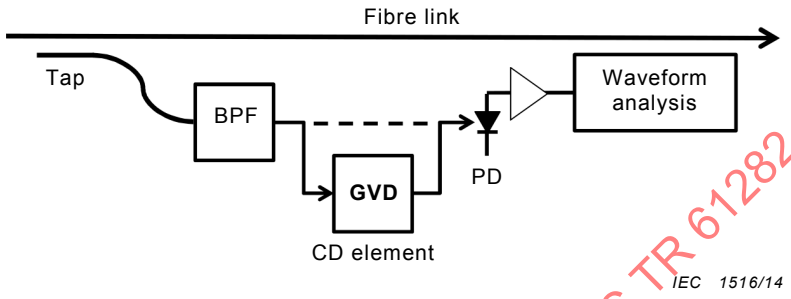

Key

BPF optical band-pass filter

GVD group velocity dispersion

PD high-speed photo-detector

Figure 12 – Set-up for determining the sign of the GVD in the fibre link with an additional optical CD element of known GVD magnitude and sign

It is important to note that photo-detectors are also sensitive to waveform distortions caused by PMD, which converts AM partially into polarization modulation and PM partially into AM or polarization modulation. Therefore, it is necessary to separate the PMD-induced waveform distortions from those induced by CD, if one wants to measure the accumulated GVD (or DGD) in a transmitted WDM signal. Hence, most methods using high-speed intensity detection have the capability to simultaneously measure accumulated GVD and effective DGD in the transmitted signal. However, the uncertainty of a GVD measurement may increase significantly when the optical signal is distorted by large PMD, and likewise, the uncertainty of a DGD measurement may be affected by large CD.

A common feature of all direct-detection methods is that the CD- and PMD-induced waveform distortions depend strongly on the modulation type and format of the signal. They are not only substantially different for OOK and PSK signals, but also vary largely between RZ and NRZ-formatted signals [6]. In addition, they are sensitive to phase or frequency chirp in the signal. Therefore, instruments based on direct-detection receivers need to be carefully calibrated, preferably with the same signal as the one analysed, or at least with a signal from a transmitter of identical design [6].

5.2.2 Asynchronous waveform sampling

This measurement technique was originally developed for NRZ- or RZ-OOK optical signals, where the transmitted optical pulses are noticeably distorted when the signal has experienced significant amounts of GVD or DGD in the fibre link. As described below, there are several methods to quantitatively characterize these waveform distortions as a function of the accumulated GVD (or DGD). It is thus possible to measure the GVD in a fibre link by comparing the observed waveform distortions in the transmitted signal with those measured in a series of calibration tests, wherein the signal is passed through optical elements with precisely known dispersion.

Optical signals with identical modulation format generally exhibit similar waveform distortions when experiencing the same amount of GVD, especially if they are generated by transmitters of identical design. Thus, it is usually not necessary to run calibration tests with each individual WDM signal transmitted through the fibre, but instead use a single set of reference measurements. Small variations in the modulation characteristics of the signals may be compensated for by training the distortion analyser with a sufficiently large number of different signal sources [6].

Recording the CD-induced waveform distortions as a continuous function of time requires complex and expensive equipment, like a real-time digitizing oscilloscope. A more compact and cost-effective solution is to sample the received electric signal periodically, using a sampling time substantially shorter than the symbol period of the digital modulation, and to collect a large number of random samples, each taken on a different transmitted pulse [19], as shown schematically in Figure 13.

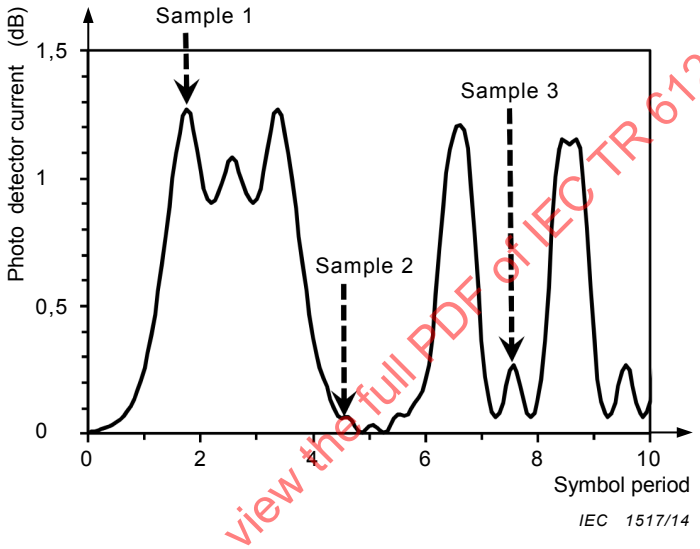

Figure 13 – Asynchronous sampling of the waveform of a 10 Gbit/s NRZ-OOK signal

It is important to note that this statistical method does not require samples to be taken rapidly in each succeeding symbol period. In fact, the sampling rate may be several orders of magnitude slower than the symbol rate. However, it is essential that the sampling rate is not synchronized with the clock frequency of the digital modulation, so that the randomly collected samples uniformly cover the entire symbol period. This asynchronous waveform analysis thus yields a distribution (or histogram) of the waveform variations integrated over the entire symbol period, in contrast to conventional, synchronously sampled eye diagrams, which provide waveform histograms for each time slot within the symbol period [19]. Nevertheless, asynchronously sampled waveform histograms contain sufficient information to detect the presence of GVD or DGD in the optical signal. As an example, Figure 14 compares the simulated histogram of a 10 Gbit/s NRZ-OOK signal without GVD or DGD with those obtained when the signal has experienced 1 000 ps/nm GVD or 48 ps DGD.

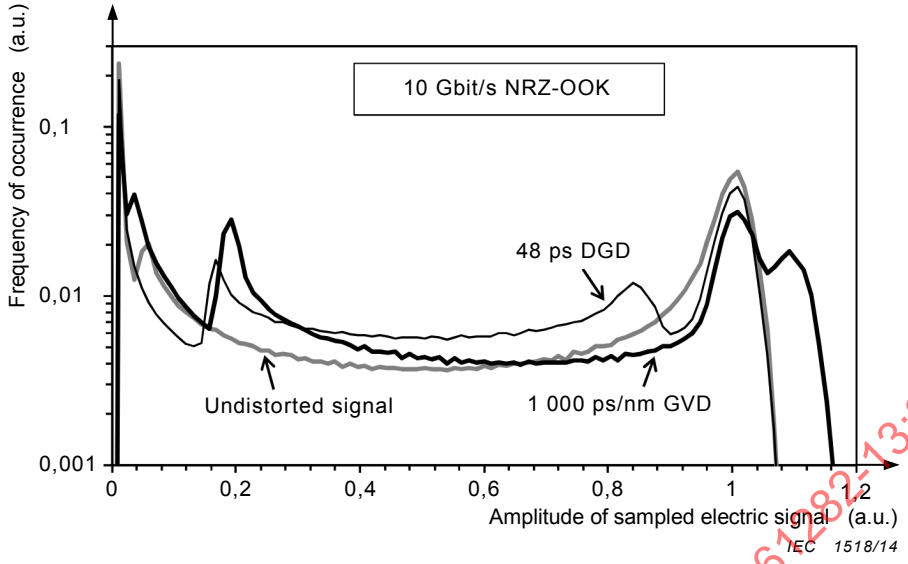

Figure 14 – Asynchronously sampled waveform histograms of a 10 Gbit/s NRZ-OOK signal without dispersion, with 1 000 ps/nm GVD, and with 48 ps DGD

The histograms of Figure 14 clearly show that the waveform distortions caused by CD differ substantially from those introduced by PMD. Therefore, CD-induced waveform distortions may be distinguished from those originating from PMD or other transmission impairments.

These differences become even more visible when collecting not just one sample from any given symbol period, but instead a pair of samples separated by a fixed time interval Δt, as shown in Figure 15. The time interval between the two samples may be equal to the symbol period [6], as shown in Figure 15, or only a fraction thereof [21].

Since the two samples of each pair are correlated, they provide far more information on the time dependence of the waveform distortion than the single-sample method described above. However, the dual-sample technique usually requires two waveform samplers operated in parallel and synchronised properly with each other, as shown in Figure 16. The requirements for the repetition rate of the dual-sample technique are the same as described above for the single-sample method.

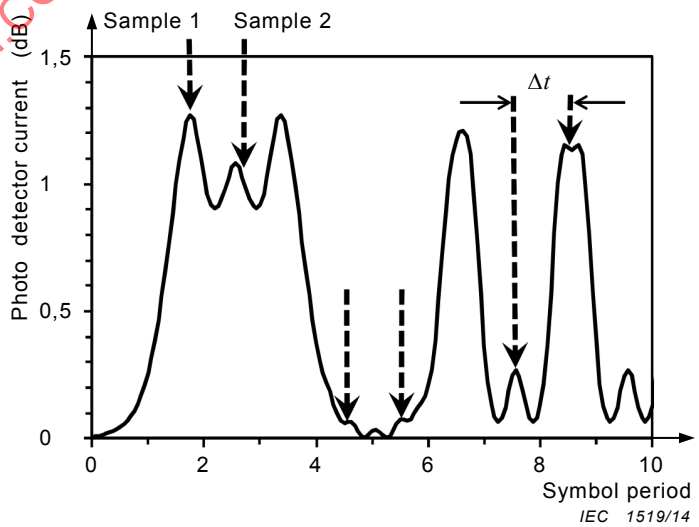

NOTE The two samples are separated by a fixed time interval Δt.

Figure 15 – Asynchronous waveform analysis with two successive samples per symbol period

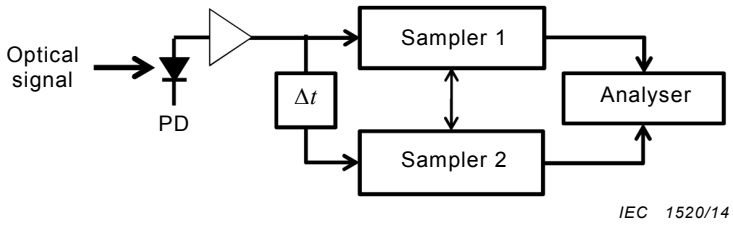

Key

PD high-speed photo-detector

Δt time delay between samples

Figure 16 – Apparatus for asynchronous waveform analysis with time-delayed dual sampling

The resulting waveform samples may then be displayed in a two-dimensional graph by plotting the amplitude of each first sample against that of the corresponding second sample, as shown in the example of Figure 17, where Δt is equal to one symbol period. When a sufficiently large number of samples is collected, these plots form relatively simple patterns, in particular for undistorted signals, which reflect the shapes of the received waveforms. It can be clearly seen in Figure 17 that these patterns become uniquely distorted when the signal experiences significant amounts of GVD and/or DGD, which can be utilized to distinguish CD-induced waveform distortions from those introduced by PMD. The patterns also change when other impairments are present in the signal, like ASE noise from optical amplifiers [6, 19].

The collected samples can be further evaluated by converting the two-dimensional plots into two-dimensional histograms, which then display the joint probability distribution of the amplitudes of the first and second sample. These two-dimensional probability functions, known as phase portraits, may then be plotted as grey-scale images of the joint probability function and analysed using digital pattern recognition techniques [6, 21]. Calibration of the instrument is a complicated procedure and involves “training” of the pattern recognition software on signals with various amounts of GVD and in the presence of other background distortions (such as CD and optical noise). After sufficient training, the software can simultaneously and independently recognise and quantify different waveform distortions in the phase portraits, thus allowing independent measurement of GVD, effective DGD, and even OSNR [6].

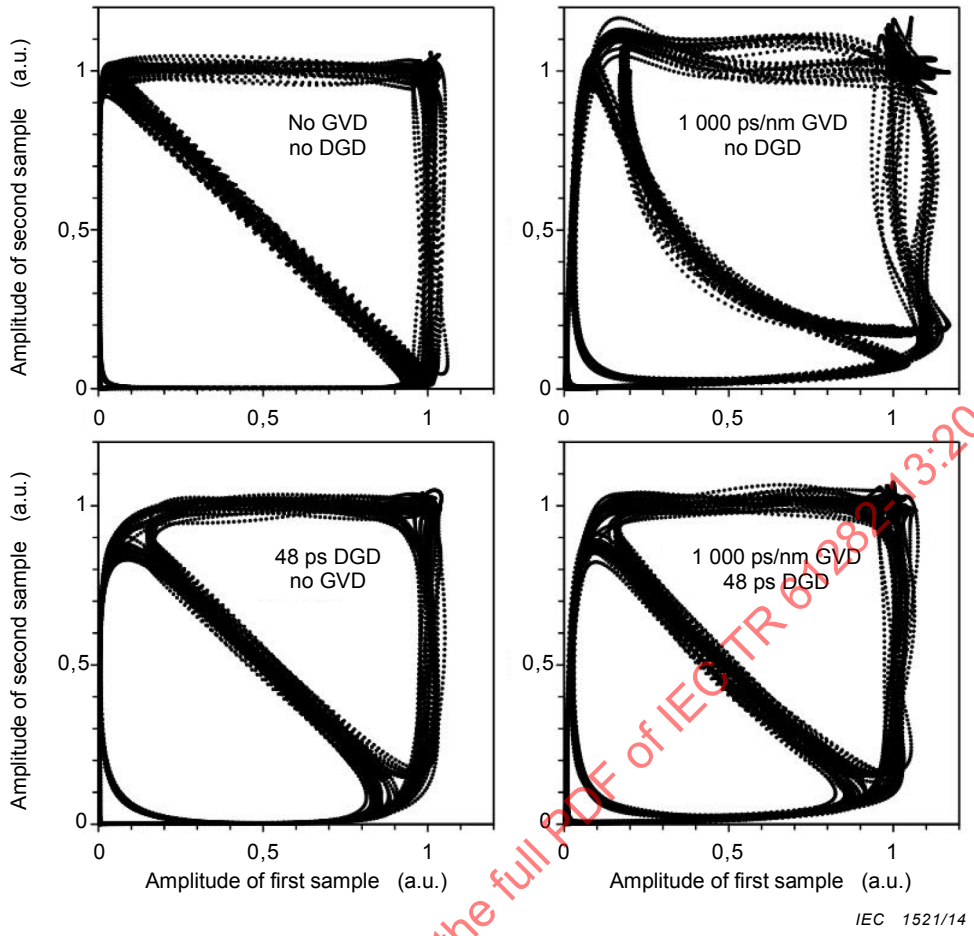

Key

DGD differential group delay

GVD group velocity dispersion

NOTE The time delay between each sample pair is equal to one symbol period.

Figure 17 – Phase portraits of a 10 Gbit/s NRZ-OOK signal with various amounts of GVD and DGD

The accuracy of these waveform analysers has been evaluated in various lab and field trials, using 10 Gbit/s NRZ-OOK signals and one-symbol time delays [22, 23]. The average random measurement uncertainty (standard deviation) was found to be about ±17 ps/nm for GVD up to 800 ps/nm and ±3 ps for effective DGD up to 24 ps [22]. Not surprisingly, the measurement accuracy degrades significantly when large background distortions from ASE noise and PMD (or CD) are present, increasing the uncertainty to about ±27 ps/nm for GVD and ±4 ps for effective DGD [22].

As clearly seen in Figure 17, phase portraits taken with a time delay of one symbol period are more sensitive to waveform distortions caused by CD than to those introduced by PMD. The sensitivity to PMD-induced distortions can be increased, at the expense of CD sensitivity, by decreasing Δt to half the symbol period [21]. This is shown in Figure 18, which displays a set of phase portraits that were calculated for the same conditions used in Figure 17 but with Δt set to half the symbol period.

Asynchronous waveform sampling may be applied to many other modulation formats and, indeed, has been utilized to measure GVD on RZ-formatted OOK signals as well as on NRZ- and RZ-formatted DPSK signals [6, 21, 24].

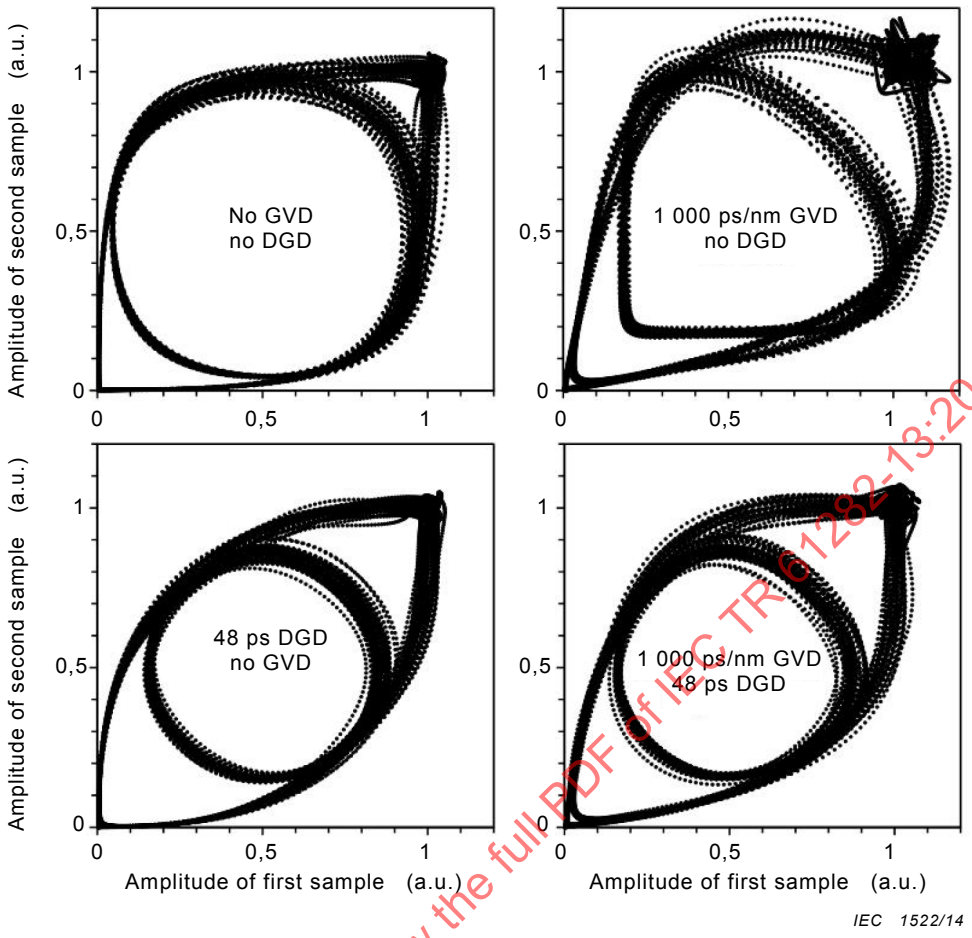

Key

DGD differential group delay

GVD group velocity dispersion

Figure 18 – Phase portraits of a 10 Gbit/s NRZ-OOK signal wherein the time delay between each sample pair is set to half the symbol period

5.2.3 RF spectral analysis

Waveform distortions in OOK signals can be readily observed in the RF spectrum of the received photo-detector current. The CD-induced partial conversion from AM to PM, for example, creates noticeable depressions (or holes) at certain frequencies in the spectrum, which are more pronounced for RZ-OOK than for NRZ-OOK signals (see Figure 19; the RZ-pulses analysed here and in Figures 20 and 21 have a 3-dB width of about 50% of the symbol period). The centre frequency of these depressions, therefore, represents a unique measure of the amount of GVD the signal has experienced.

Another unique feature observed in the RF spectrum of NRZ-OOK signals is the appearance of a relatively strong frequency component at the clock frequency of the digital modulation with increasing GVD, which is not present in the undistorted signal [19]. This clock frequency component rises rapidly with increasing GVD until it reaches a maximal value, after which it decreases with increasing GVD, as shown in Figure 20. It may thus be utilized to measure GVD in a transmitted signal [19].

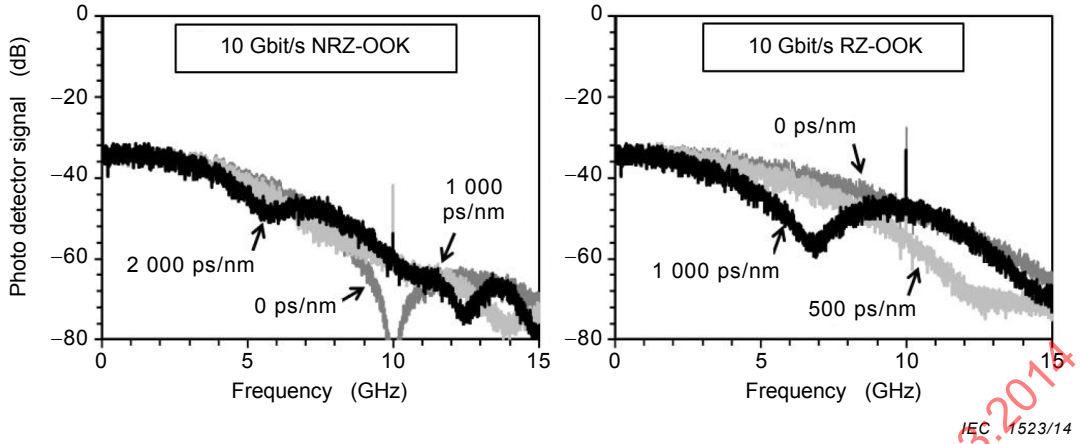

Figure 19 – RF spectra of directly detected 10 Gbit/s NRZ- and RZ-OOK signals distorted by various amounts of GVD

However, the periodic variation of this signal with GVD severely limits the range over which GVD can be measured unambiguously (to about 800 ps/nm with 10 Gbit/s signals). Moreover, the strength of the clock frequency component depends not only on the GVD the signal has experienced but also quite sensitively on the shape of the transmitted optical pulses [18]. Thus, careful calibration is required when deriving GVD from clock frequency measurements.

For RZ-OOK signals, the clock frequency component is maximal in the absence of CD and decreases slowly with increasing GVD until it reaches a steep minimum and increases again. Hence, the range over which GVD can be measured unambiguously is also very limited (to about 650 ps/nm).

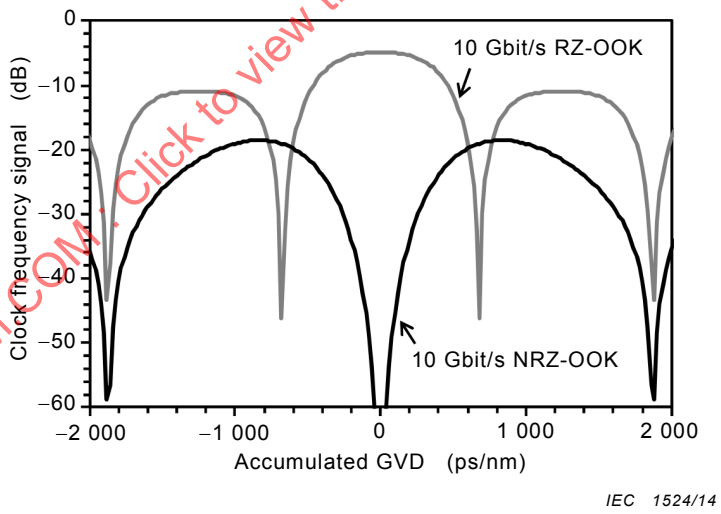

Figure 20 – Magnitude of the clock frequency component in the RF spectra of 10 Gbit/s NRZ- and RZ-OOK signals as a function of GVD

Moreover, the presence of PMD in the fibre link may cause additional depressions in the RF spectrum, as shown in Figure 21, which can severely impair the GVD values deduced from the magnitude of the clock frequency component [19]. Thus, a single receiver is usually not sufficient to obtain the GVD from a spectral analysis of the photo-detector current.

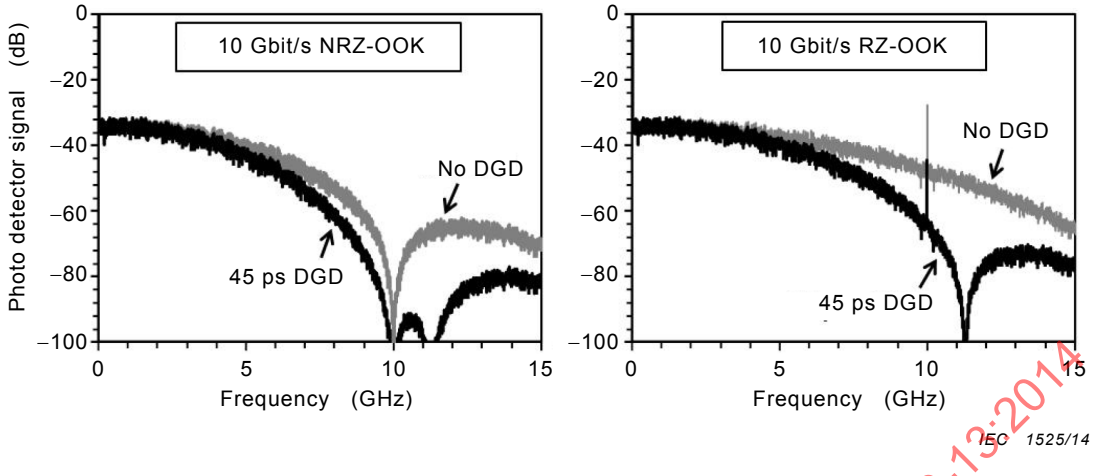

Figure 21 – Impact of PMD on the RF spectra of directly detected 10 Gbit/s NRZ- and RZ-OOK signals

For NRZ- and RZ-OOK signals, the detrimental effects of PMD on GVD measurement can be avoided by splitting and filtering the optical signal in such a way that the upper and lower modulation sidebands of the optical spectrum are detected separately by two parallel receivers [3, 25], as shown in Figures 22 and 23.

As a result, the beat frequency of the optical carrier with the clock frequency component in the upper modulation sideband is detected in one of the receivers and the beat frequency of the carrier with the clock frequency component in the lower modulation sideband in the other receiver. The magnitude of these two beat frequencies then depends only on the DGD in the signal, whereas their relative phase depends only on the GVD. Thus, the GVD in the signal can be calculated from the electrical phase difference, $\Delta\phi$, between the two clock frequency beat signals, which is given by [3, 4],

$$\Delta\phi = 2\pi D(\lambda) L_f \lambda^2 f_{\text{clock}}{}^2 / c \tag{13}$$

wherein f_{clock} denotes the clock frequency, while the effective DGD, $\Delta\tau_{eff}$, can be determined independently from the magnitude of the beat signals, which varies with DGD as

$$\cos^2\left(\pi f_{\text{clock}} \Delta\tau_{eff}\right) \tag{14}$$

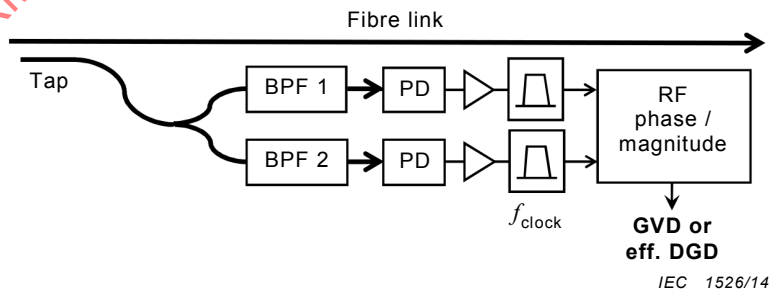

Key

BPF optical band-pass filter

PD high-speed photo-detector

f_{clock} electrical band-pass filter for clock frequency component

Figure 22 – Apparatus for simultaneous GVD and DGD measurements on NRZ- or RZ-OOK signals using separate detectors for upper and lower modulation sidebands

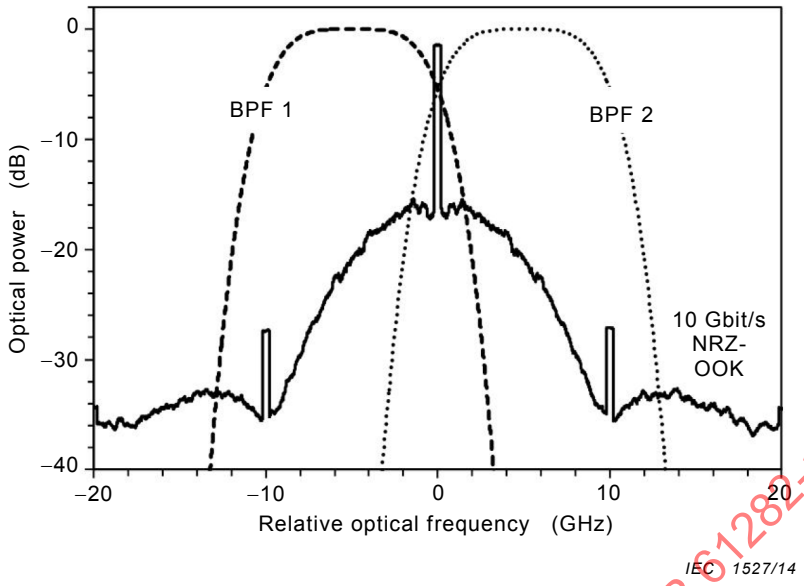

Key

BPF optical band-pass filter

Figure 23 – Optical filtering of a 10 Gbit/s NRZ-OOK signal for separate detection of upper and lower modulation sidebands

It is important to note that Equation (13) provides information not only on the magnitude of the GVD but also on its sign. The accuracy of the GVD measurement depends on the precision of the electrical phase measurement and generally increases with the symbol rate of the signal, i.e. with f_{clock}. With a 40 Gbit/s NRZ-OOK signal, GVD of up to 4 742 ps/nm has been measured with an average random uncertainty (standard deviation) of ±100 ps/nm and effective DGD of up to 200 ps with an uncertainty of ±4 ps/nm, even in the presence of relatively large ASE noise (10 dB OSNR) [3]. For precise GVD measurements, detailed knowledge of the exact symbol rate of the signal is required, whereas the optical pulse shape is important for precise measurements of the effective DGD.

Although the modified spectral analysis method works well with conventional NRZ- and RZ-formatted OOK signals, it is not applicable to many other modulation formats, since it requires a relatively strong carrier frequency component as well as two distinct (clock) frequency components to be present in the optical spectrum of the signal. For example, the method does not work with carrier-suppressed RZ-OOK (CSRZ-OOK) or NRZ- / RZ-PSK signals, which do not exhibit a strong carrier frequency component.

5.3 CD and PMD measurements based on high-speed coherent detection

5.3.1 Introductory remark

High-speed coherent receivers are increasingly employed in WDM transmission systems operating at bit rates of 40 Gbit/s and above to demodulate the transmitted signal and to remove signal distortions caused by CD and PMD. These receivers can also be used to measure the accumulated GVD and DGD in the received signal, because they transform the properties of the received optical signal into the electrical domain, where they can be readily analysed using well established electronic techniques.

Another important method is based on adaptive compensation of the accumulated GVD and DGD in the coherently received electrical signals. This method has become feasible with the recent advent of high-speed digital signal processors, which can introduce, and hence compensate, large amounts of GVD and DGD in the electronic signals. Thus, the accumulated GVD (or DGD) in the received optical signal can be measured by varying the setting of the electronic compensator until the CD- (or PMD-) induced signal distortions are minimized.

Thus, GVD and DGD can be directly determined from the settings of the compensator. However, this method requires precise knowledge of the signal's modulation format and symbol rate.

5.3.2 Heterodyne detection

A simple heterodyne receiver, where the local oscillator laser is tuned to a frequency outside of the modulation bandwidth of the received optical signal, can be used to implement the modified spectral analysis method described in 5.2.3. Since heterodyning transforms the spectrum of an optical signal directly into an electrical spectrum, as shown in Figure 24, the desired beating of the carrier component with the two clock frequency components can be obtained by electrical filtering and mixing of the received photo-detector signals [4]. By using narrow-band electrical filters, which are readily available, the resulting beat signals are much cleaner than in the case of optical mixing in a photo-detector, thus improving the precision of the phase measurement. Furthermore, the effective DGD in the signal can be directly measured by varying the polarization state of the local oscillator laser relative to that of the signal, irrespective of the magnitude of the clock frequency components [4].

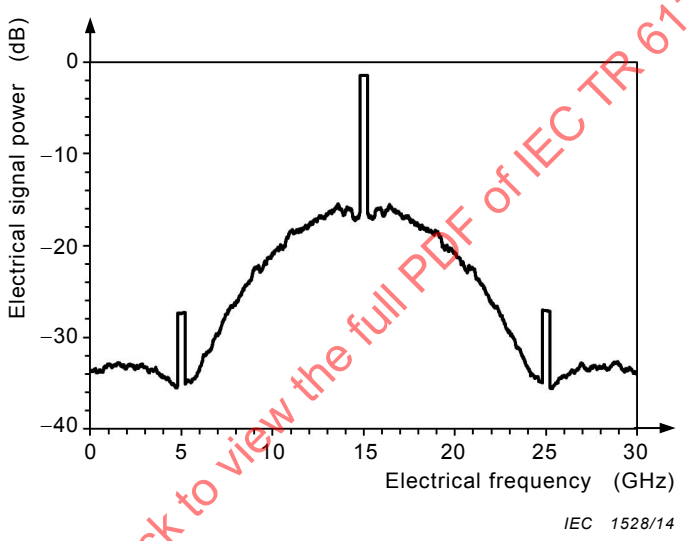

Figure 24 – RF power spectrum of a 10 Gbit/s NRZ-OOK signal detected with an optical heterodyne receiver

However, the electrical bandwidth of the photo-detectors used in heterodyne receivers needs to be much higher than the clock frequency of the signal to be analysed (about 2,5 times higher in the example of Figure 20), which makes it quite difficult to implement these receivers for symbol rates much higher than 10 GBd.

5.3.3 Direct detection with optical CD or PMD compensation

5.3.3.1 GVD measurements via CD compensation

A generally applicable method for measuring CD in a fibre link is to adaptively compensate the GVD experienced by the signal. This compensation may be performed in the optical domain, as shown in Figure 25, or electronically in a coherent receiver, as described below. In any case, implementation of this technique requires a calibrated tuneable dispersion compensator (or dispersion emulator) and a high-speed dispersion monitor connected to the output of the compensator. The purpose of the dispersion monitor is to detect residual distortion in the output the compensator and to provide feedback to the compensator. The GVD in the compensator is then automatically adjusted until the CD-induced signal distortions in the output of the compensator are minimal. When this minimum is reached, the GVD in the compensator is equal in magnitude to the GVD in the fibre link but opposite in sign.

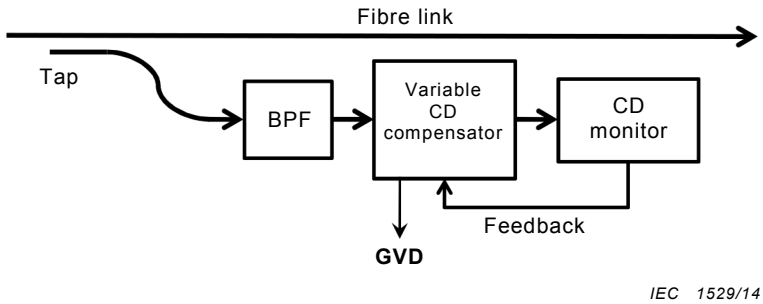

Figure 25 – Apparatus for measuring GVD with calibrated optical CD compensator

5.3.3.2 DGD measurements via PMD compensation

Very similarly, accumulated DGD in a transmitted WDM signal may be measured by using a calibrated adaptive optical PMD compensator to remove the PMD-induced distortions from the received optical signal [11, 12]. In this case, the variable CD compensator is replaced by an adjustable first-order PMD emulator and the CD monitor by a suitable optical PMD analyser (PMD Monitor 1), as shown schematically in Figure 26. The variable PMD emulator may consist, for example, of an adjustable polarization controller followed by an adjustable polarization-dependent differential delay line (DGD compensator), or may even generate variable combinations of first- and higher-order PMD.

The PMD monitor may be a high-speed optical receiver which measures the waveform distortions in the receive signal, as described above in 5.2.2 and 5.2.3, or, in the case of single-polarized signals, it can be a spectrally wideband optical polarimeter that measures the signal's degree of polarization (DOP) of the entire analysed signal [11, 12]. It is well known that the DOP of a single-polarized signal is maximal when the PMD-induced distortions are minimal and that the DOP decreases when the PMD-induced distortions increase.

In either case, the amount and orientation of the DGD generated by the PMD emulator is then automatically adjusted until the PMD-induced signal distortions in the output of the emulator are minimal, e.g. until the DOP of the output signal is maximal [11, 12]. It should be noted that it is not necessary to measure the exact absolute value of the DOP in order to adjust the DGD in the PMD emulator. Rather, it is sufficient to measure the relative value of the DOP, because the DGD in the fibre link is measured when the DOP is maximal. For this reason, the DGD measurement does not depend on the signal's modulation format and spectral width, even though the sensitivity of the DOP to DGD varies with the signals' modulation format and spectral width.

When this condition is reached, the DGD generated by the PMD emulator is equal to the DGD in the fibre link. Hence, when the variable DGD element in the PMD emulator is properly calibrated it indicates the instantaneous DGD $\Delta\tau$ used to compensate the PMD-induced distortion in the analysed signal, and not just the effective DGD $\Delta\tau_{eff}$ like the methods described in 5.1. However, it should be noted that it is usually impossible to measure $\Delta\tau$ when the launch SOP is equal or close to one of the two input PSPs of the fibre link [12]. In fact, when the analysed signal is launched in one of the PSPs of the fibre link and subsequently passes the PMD-emulator in one of its PSPs, then the DGD in the PMD emulator may assume arbitrary values without changing the distortion in the analysed signal.

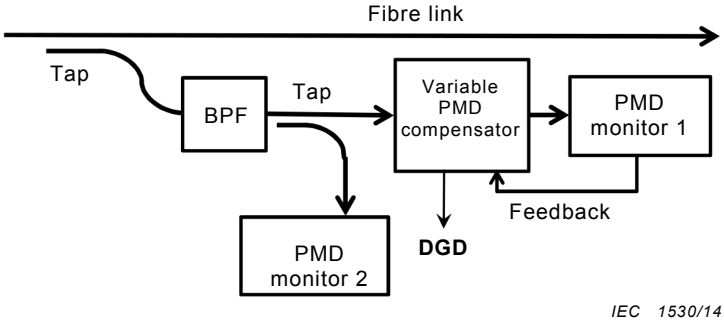

Figure 26 – Apparatus for measuring PMD with calibrated optical DGD compensator

Consequently, DGD readings from the PMD-emulator are unreliable when the launch SOP of the analysed signal is equal or close to one of the PSPs of the fibre link. Therefore, DGD measurements taken under these conditions have to be identified and removed from the ensemble of measurements which are used to calculate the mean DGD. This may be achieved by inserting a second PMD monitor before the PMD-emulator to estimate the PMD-induced distortions in the uncompensated signal (PMD Monitor 2 in Fig. 26) [11,12]. When the signal distortion before the PMD-emulator is low and the DGD reported by the emulator is high, then the analysed signal was likely transmitted in one of the PSPs of the fibre link. However, the situation is less clear when the distortion before the PMD-emulator and the DGD reported by the emulator are both low. Under these circumstances, one may inadvertently remove a valid (although low) DGD reading from the ensemble of measurements, thus introducing an undesired bias in the measurement ensemble towards higher DGD values.

However, it should be noted that the instantaneous DGD at the optical frequency, where the signal is transmitted in one of the PSPs of the fibre link, may be measured at a later time when the signal's launch SOP is no longer identical or close to either of the two PSPs, since the PSPs of the fibre link and even the launch SOP of the signal usually vary with time.

The decision about the validity of a DGD reading is further complicated by the fact that the sensitivity of the PMD monitors usually varies considerably with the modulation format and bit rate of the analysed signals. For example, the DOP of a conventional NRZ- or RZ-OOK signal is less sensitive to PMD-induced distortions than that of a (carrier-suppressed) BPSK or QPSK signal. Furthermore, the DOP of spectrally broadband (i.e. high-baud-rate) signals is more sensitive to PMD-induced signal distortions than that of narrowband signals. Therefore, the PMD monitor needs to be carefully calibrated with the specific modulation format and bit rate of the analysed signal, so as to obtain accurate PMD measurements.

For these reasons, the method is most reliable when used with spectrally broadband and well defined probe signals, rather than with commercial traffic signals of potentially unknown modulation formats and bit rates [12].

5.3.4 Electronic CD and PMD compensation in intradyne coherent receiver

Although the CD and PMD compensation methods may be implemented with tuneable optical emulators, as described above in 5.3.3.1 and 5.3.3.2, a more compact solution is to use a coherent optical receiver with high-speed digital signal processing, where CD and PMD can be compensated numerically in the electronic domain, as shown schematically in Figure 27. Modern coherent receivers, designed for applications in commercial WDM transmission systems, employ complex optical mixers with phase and polarization diversity and generate four electrical output signals which carry all information on the signal's amplitude, phase, and polarization state, even when the local-oscillator laser is tuned close to the centre frequency of the received signal (known as "intradyne" detection). Therefore, it is possible to compensate linear transmission impairments experienced by the optical signal, such as CD and PMD, after the signal has been detected and converted into electronic signals [26]. This

impairment compensation is usually performed in a high-speed digital signal processor (DSP), using specially developed numerical algorithms.

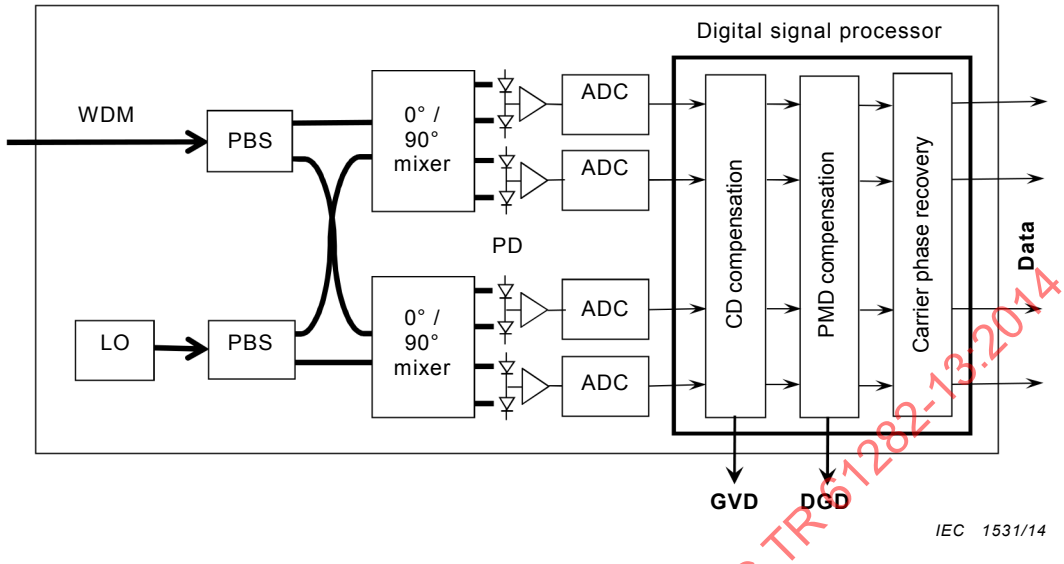

Key

LO local oscillator laser

PBS polarization beam splitter

PD high-speed photo-detector

ADC high-speed analogue-to-digital converter

Figure 27 – Coherent optical receiver with high-speed digital signal processing and electronic CD and PMD compensation

These feedback-based algorithms essentially perform the same functions as optical CD or PMD compensators, i.e. they generate variable GVD and DGD in the digitised electrical signals and automatically adjust their amounts until the quality of the equalised signals is optimal [26]. Because the compensation is a numerical process, the amounts of GVD and DGD introduced in the equalised signals can be precisely determined from the settings of the compensators. Hence, they can be used to measure GVD and instantaneous DGD in the fibre link. However, the algorithms in the DSP need to be customised to the particular modulation format of the transmitted signal.

A unique feature of this numerical signal processing is that the compensation range can be much larger than that of analogue optical compensators (e.g. up to 50 000 ps/nm GVD). However, the precision with which GVD and DGD can be determined depends strongly on the sensitivity of the transmitted signal to CD and PMD. A commercial coherent receiver for 40 Gbit/s polarization-multiplexed QPSK signals, tested under various operating conditions, was found to be capable of measuring GVD of 2 890 ps/nm in the fibre link with an average random uncertainty (standard deviation) of ±60 ps/nm as well as link DGD between 10 ps and 123 ps with an uncertainty of ±5 ps [27].

It should be noted that these coherent receivers are frequently employed to detect polarization-multiplexed QPSK signals (e.g. at 40 Gbit/s and 100 Gbit/s line rates), wherein the optical phase of each polarization tributary is digitally modulated and varies between four discrete values. The SOP of such signals thus passes rapidly (and randomly) through four different polarization states: two pairs of mutually orthogonal SOPs, wherein the two SOPs of the second pair are 50/50 combinations of the SOPs of the first pair. Therefore, even if one of these pairs coincides with the two PSPs of the fibre link, the other pair of SOPs is launched in a 50/50 mix of the two PSPs. As a result, the DGD in the electronic PMD emulator can always be adjusted unambiguously to match that of the fibre link. Thus, unlike in the case of single-

polarized signals (see 5.3.3.2) the DGD readings from the electronic PMD emulator are always reliable.

Because of the high wavelength selectivity of coherent detection, there is usually no need for preceding the receiver with a tuneable channel selection filter, as is required for direct-detection analysers. GVD and DGD measurements may be performed by connecting the instrument directly to the fibre link [2].

6 Semi-intrusive fibre characterization with special probe signals

6.1 CD measurement using multi-tone probe signal

6.1.1 Introductory remark

End-to-end CD in deployed fibre links is usually determined from measurements of the relative group velocity of a multitude of optical signals which are transmitted simultaneously through the fibre link at different wavelengths. To facilitate this measurement, the amplitude of all launched optical signals is modulated simultaneously with a periodic signal of predetermined frequency. A group velocity difference between any two of the transmitted signals then causes a differential time delay (or phase shift) in the amplitude modulation of the signals at the output end of the link, which can be readily measured with the help of an electronic phase meter. This technique is known as the differential phase shift method (see IEC 60793-1-42).

CD test instruments often employ a broadband modulated light source, in which one of the wavelengths serves as the reference signal for the differential phase shift method. The broadband light source allows group velocity dispersion measurements over a fairly wide optical bandwidth. However, it requires that the entire fibre link has to be taken out of service for the duration of the measurement.

The differential phase shift method may be adopted for in-service fibre characterization by using narrowband optical probe signals which can be transmitted through unused WDM channels [9]. In this case, the probe signals have to be analysed separately for each WDM channel, as described in more detail in the following subclauses.

6.1.2 Differential phase shift method with narrowband probe signals

6.1.2.1 Probe signals with two frequency tones

When employing the differential phase shift method, at least two optical signals at different wavelengths have to be transmitted simultaneously through the fibre link to allow measurement of the group velocity dispersion $D(\lambda)$ at a desired wavelength λ. The two signals may be spaced sufficiently close in wavelength to be transmitted through a single WDM channel, as shown in Figure 28. Group velocity dispersion in the fibre link introduces a differential time delay Δt between the two optical signals, which is given by [3, 4]

$$\Delta t = D(\lambda)\, L_f\, \lambda^2\, \Delta f / c \qquad (15)$$

wherein Δf denotes the frequency separation of the wavelengths, L_f the length of the fibre link, and c the speed of light.

Measurement of the differential time delay at the output end of the fibre link requires that the two wavelengths carry unique time markers, e.g. in the form of a common sinusoidal amplitude modulation at frequency F which is simultaneously imposed on the two signals before they are launched into the link. In this case, the differential time delay Δt can be observed as a differential phase shift $\Delta\phi$ in the amplitude modulation of the received signals at the end of the fibre link. A suitable signal analyser for measuring this differential phase shift

is shown in Figure 29. It employs an optical diplexer to separate the two frequency tones and direct them to two parallel photo-detectors, which are connected to the phase meter. The maximal differential time delay Δt_{max} which can be measured in this way is limited by the time period of the amplitude modulation, i.e. $\Delta t_{max} < 1/F$.

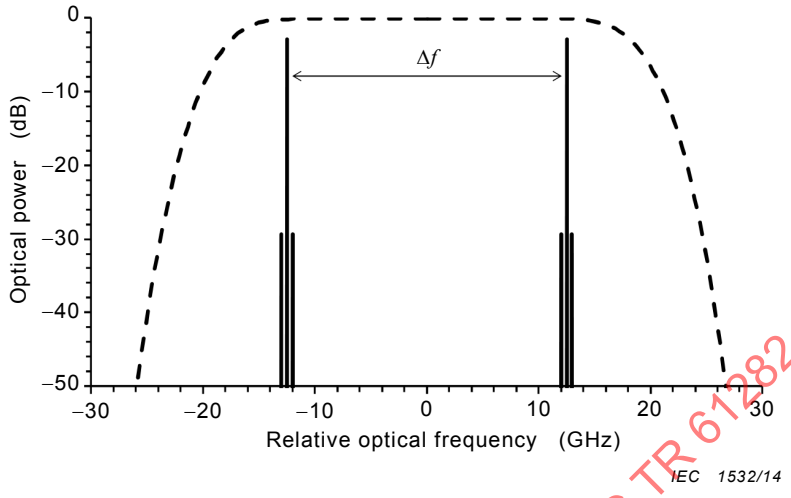

NOTE The dashed curve shows a typical transmission window of a 50-GHz wide WDM channel.

Figure 28 – Spectrum of an amplitude modulated dual-wavelength probe signal

The two wavelengths of the probe signal may be generated by a pair of two frequency-locked lasers, as shown in Figure 29. However, it is important that the frequency separation Δf is precisely maintained at the desired value, because the measured time delay Δt is directly proportional to Δf (see Equation (15)). To achieve a measurement accuracy of less than 1 % with a frequency spacing of Δf = 25 GHz, for instance, the frequency separation of the two lasers has to be maintained within 250 MHz, which requires precise frequency locking of the two lasers.

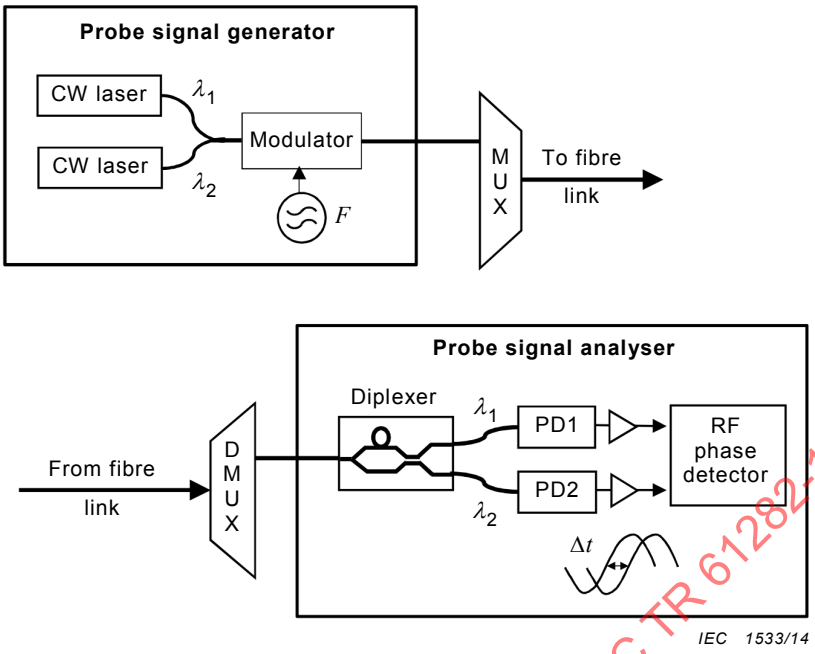

Key

CW	continuous wave
MUX	WDM multiplexer
DMUX	WDM demultiplexer
PD	photo-detector

Figure 29 – Signal generator and analyser for dual-wavelength probe signal

Two wavelengths with precisely maintained frequency separation may be generated from a single CW laser by means of a high-speed optical amplitude modulator, as shown in Figure 30. A high-speed Mach-Zehnder modulator is operated around a point of maximal carrier suppression and simultaneously driven with two sinusoidal electrical signals of slightly different frequencies f_1 and f_2 [10]. This modulation produces two pairs of wavelengths which are spaced by $\Delta f = 2f_1$ and $\Delta f = 2f_2$, respectively. This four-wavelength probe signal does not require additional amplitude modulation, because the four wavelengths produce two phase-correlated beat signals at frequency $| f_1 - f_2 |$ in the photo-detector currents of the signal analyser.

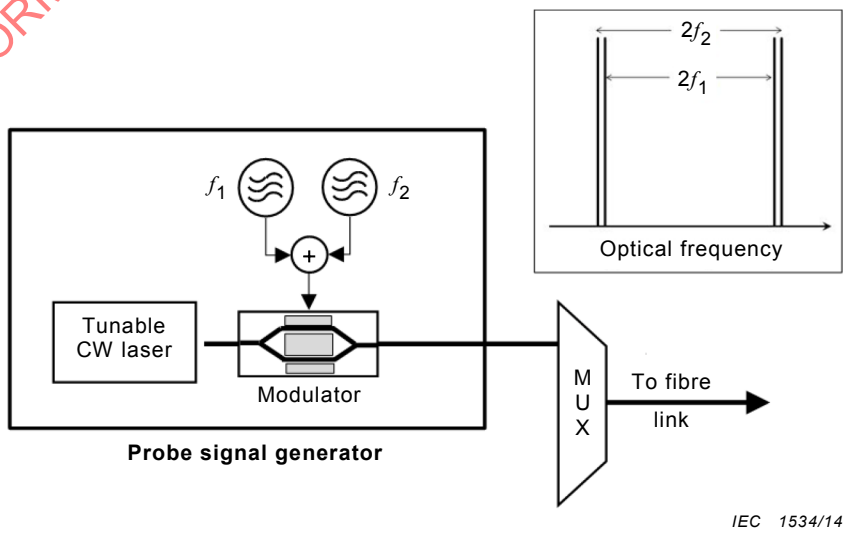

Figure 30 – Four-wavelength probe signal generator using high-speed modulator